(4)

A TRIDENT SCHOLAR PROJECT REPORT

NO. 171

"ON THE BREAKDOWN OF A VORTEX"

UNITED STATES NAVAL ACADEMY
ANNAPOLIS, MARYLAND

UNCLASSIFIED

SECURITY CLASSIFICATION OF THIS PAGE *(When Data Entered)*

REPORT DOCUMENTATION PAGE		READ INSTRUCTIONS BEFORE COMPLETING FORM
1. REPORT NUMBER U.S.N.A. - TSPR; 171 (1990)	2. GOVT ACCESSION NO.	3. RECIPIENT'S CATALOG NUMBER
4. TITLE *(and Subtitle)* ON THE BREAKDOWN OF A VORTEX.		5. TYPE OF REPORT & PERIOD COVERED Final 1989/90
		6. PERFORMING ORG. REPORT NUMBER
7. AUTHOR*(s)* Douglas E. Reckamp		8. CONTRACT OR GRANT NUMBER*(s)*
9. PERFORMING ORGANIZATION NAME AND ADDRESS United States Naval Academy, Annapolis.		10. PROGRAM ELEMENT, PROJECT, TASK AREA & WORK UNIT NUMBERS
11. CONTROLLING OFFICE NAME AND ADDRESS United States Naval Academy, Annapolis.		12. REPORT DATE 22 May 1990 13. NUMBER OF PAGES 89
14. MONITORING AGENCY NAME & ADDRESS*(if different from Controlling Office)*		15. SECURITY CLASS. *(of this report)* 15a. DECLASSIFICATION/DOWNGRADING SCHEDULE

16. DISTRIBUTION STATEMENT *(of this Report)*

This document has been approved for public release; its distribution is UNLIMITED.

17. DISTRIBUTION STATEMENT *(of the abstract entered in Block 20, if different from Report)*

18. SUPPLEMENTARY NOTES

Accepted by the U.S. Trident Scholar Committee.

19. KEY WORDS *(Continue on reverse side if necessary and identify by block number)*

Vortex-motion
Vortex generators
Laser Doppler velocimeter
Fluid dynamics

20. ABSTRACT *(Continue on reverse side if necessary and identify by block number)*

The physical problem presented in this paper is water rotating steadily in a vertical cylinder with a specified tangential influx. Water is withdrawn through a sink in the center of the base of the cylinder. Laser Doppler velocimetry is utilized to obtain velocity data in and near the viscous vortex core region, the viscous boundary layer, and the near irrotational region. Of particular interest is the

(OVER)

DD FORM 1 JAN 73 1473 EDITION OF 1 NOV 65 IS OBSOLETE

S/N 0102-LF-014-6601

UNCLASSIFIED

SECURITY CLASSIFICATION OF THIS PAGE *(When Data Entered)*

region near the sink where the viscous core interacts with the bottom boundary layer. The core radius is measured for various circulations with fixed sink radius and water column depth. Tangential and axial velocity measurements are taken through the viscous core and into the near irrotational region for various circulations with fixed sink radius and water column depth and at various radial and axial locations. Axial and tangential velocities are measured near and in the bottom boundary layer. A flow visualization technique is developed to display qualitative data on the flow where the boundary layer and viscous core interact.

"ON THE BREAKDOWN OF A VORTEX"

A Trident Scholar Project Report

by

Midshipman First Class Douglas E. Reckamp 1990

U.S. Naval Academy

Annapolis, Maryland

Professor Robert A. Granger
Mechanical Engineering Department

Associate Professor Gerald Hall
Aeronautical Engineering Department

Accepted for Trident Scholar Committee

Chairperson

22 May 1990
Date

ABSTRACT

The physical problem presented in this paper is water rotating steadily in a vertical cylinder with a specified tangential influx. Water is withdrawn through a sink in the center of the base of the cylinder.

Laser Doppler velocimetry is utilized to obtain velocity data in and near the viscous vortex core region, the viscous boundary layer, and the near irrotational region. Of particular interest is the region near the sink where the viscous core interacts with the bottom boundary layer. The core radius is measured for various circulations with fixed sink radius and water column depth. Tangential and axial velocity measurements are taken through the viscous core and into the near irrotational region for various circulations with fixed sink radius and water column depth and at various radial and axial locations. Axial and tangential velocities are measured near and in the bottom boundary layer. A flow visualization technique is developed to display qualitative data on the flow where the boundary layer and viscous core interact.

ACKNOWLEDGMENTS

I would like to thank the following people for their support in helping me complete my Trident Research:

David Fry from David Taylor Research Center in Carderock Maryland provided invaluable instruction on the use of the laser Doppler Velocimeter which accelerated my data acquisition immensely. The equipment that he made available made data collection possible in the first place.

Robert Woody from the Mechanical Engineering portion of the Technical Support Division made the acquisition of a vortex generator and its subsequent modification into a useful piece of equipment possible.

Bowie Smith, the Aeronautical Engineering Laboratory Supervisor provided an open and flexible atmosphere in which to complete my research.

Finally, my Trident advisors, professors Granger and Hall whose guidance gave the theoretical background behind this complex, classical problem in fluid dynamics. They provided a foundation for meaningful research that would provide a significant contribution to the eventual solution of the problem.

TABLE OF CONTENTS

INTRODUCTION

Vortices are a widely experienced phenomenon in both the field of fluid fynamics and in everyday life. Vortex flows can be seen in hydro-machinery, centrifugal pumps, turbines, flow over submarine control surfaces, and flow over aircraft wings. When the steady vortex is disturbed, it breaks down. The precise mechanism of this vortex breakdown is one of the classical unknown problems in the field of fluid dynamics. One example of a practical application of this research is leading edge vortex formation on a delta wing. The amount of lift provided by a given wing can be increased by inducing vortices as the flow passes over the front of the wing as shown in Figure 1 of Appendix A. These vortices can break down somewhere downstream of their formation. At present, there is no reliable theory that can determine where that breakdown will occur. This research will provide data and observations that could lead to the development of such a theory.

There are three schools of thought regarding the

physical mechanism of vortex breakdown. The breakdown formation could be as a result of an instability, a critical flow situation, or a stagnation or separating flow. We have approached this experimental investigation as if the breakdown is a critical flow situation.

The rationale behind approaching the phenomenon as a critical flow is that it bears such a similarity to the critical flow situation of a hydraulic jump. The similarities are discussed later in this report.

This report is concerned with the particular case of a vortex formed in a cylindrical tank of water having a tangential influx of water and a sink located in the center of the bottom. This setup allows the experimenter to control the circulation through the use of an external valve between the pump discharge and the header. Figure 2 in Appendix A is a schematic of the system. In this application, the vortex breakdown can be initiated by simply closing then opening the flow at the sink. With the sink closed, the relatively high axial velocities of the steady flow in the core have nowhere to go and the vortex forms a complicated transient structure. The

objective of this investigation is to shed some light on the flow situation involved in this breakdown and thereby give some support to one of the theories describing the mechanism of the breakdown formation.

In order to do this, the flow parameters of the steady vortex must be fully understood and mapped out. Granger, refs 1 & 2, does this for all regions of the flow except at the boundary layer. This boundary layer is of the utmost importance since it has a major effect in the area of the formation of the breakdown. The area surrounding the core in the region of the vortex away from the bottom plate differs from that near the boundary layer where the breakdown is formed in that there are substantial viscous effects and radial velocities in the boundary layer. These viscous effects and radial velocities are not present in the region away from the plate.

This project utilizes laser Doppler velocimetry (LDV) to obtain measurements of the velocity field. Measurements are taken throughout the viscous core and free vortex region in order to refine the measurement technique and substantiate Granger's findings for this particular experimental apparatus. The core radius is

then determined for three different circulations. Velocity measurements are taken in the boundary layer region near the bottom plate.

The LDV system utilized is the Thermal Systems Incorporated 9400 system. This arrangement uses a three beam, two component LDV operated in the backscatter mode. The two velocity components measured by the LDV are at approximately 45 degrees from the vertical. The data are resolved into tangential and axial components. The backscatter mode is used in order to simplify the traversing of the beams. This method results in a lower data rate than the forward scatter mode, but allows massive amounts of data to be collected with relative ease. An automated traverse is accomplished with a TSI Mirror Mount Traverse Table. A photograph of the setup is shown in Figure 3 in Appendix A.

Objective

The objective is to collect data and make qualitative observations that can be used to substantiate the physical mechanism involved in vortex breakdown.

Coordinate Reference

In this report, cylindrical coordinated will be referenced with regard to locations within the vortex generator. The axial locations, z, are a reference to the vertical distance from the bottom plate (the bottom of the cylinder in Figures 2 and 3). Radial locations, r, are referenced to a zero at the centerline of the vortex. Negative values of r refer to the other side of the centerline (the left side in Figure 3). The positive azimuthal direction is counterclockwise when the vortex generator is viewed from the top.

Theory

The flow situation of hydraulic jump has its criticality defined by the Froude number, Fr. The Froude number is defined as follows:

$$Fr = V/\sqrt{gh} \qquad \ldots 1)$$

where

V is the free stream velocity
h is the height of the flow
and g is the acceleration due to gravity

A diagram of the hydraulic jump phenomenon is Figure 4 in Appendix A.

The Froude number determines criticality for an open channel, two dimensional, translational flow. In the situation of an internal flow vortex breakdown, a critical parameter would have to deal with closed channel, three dimensional flow having both translation plus rotation. The Froude number depends on terms that roughly deal with the speed of the flow (velocity) and its geometry (height).

The rotational strength of a vortex is governed by its circulation. The circulation is related to vorticity by the following:

$$\Gamma = \int_A \zeta \cdot dA \qquad \ldots 2)$$

The vorticity is related to the velocity by

$$\vec{\zeta} = \vec{\nabla} \times \vec{V} \qquad \ldots 3)$$

Since the following assumptions

$$\vec{V} = v_r \vec{e}_r + v_\theta \vec{e}_\theta + v_z \vec{e}_z \qquad \ldots 4)$$

(v_r and v_z: neglect; $\to 0$)

hold outside of the core radius, the vorticity becomes a function of azimuthal velocity only. The validation behind this assumption is seen in the data taken outside the vortex core. An illustration can be seen in Figure 5 of Appendix A. While the flow is outside the center region of the vortex, the dominant velocity component is in the azimuthal direction.

In order to determine an equivalent Froude number for confined vortex flow, equivalent terms that will

be used in an equation for such a non-dimensional parameter must be determined. The circulation in a vortex is roughly equivalent to the velocity in an open channel flow. There remains a length term in the open channel Froude number that must have an equivalent in the confined vortex. Equation 2) contains such a length term in that it is the integral over the area. A schematic visualization of the vortex breakdown (Figure 6 of Appendix A) suggests that the area of interest is probably the cross sectional area of the core of the vortex.

If the vortex were idealized as solid body rotation in the core region and irrotational flow everywhere outside of the core radius, then the plot of vorticity vs. radius would look like the step function on Graph 1 of Appendix B. A real vortex would have an expected vorticity vs. radius curve similar to the curved line of Graph 1. The radial location of the inflection point of this curve corresponds to the core radius, and the maximum value of vorticity is such that the average vorticity through the core is the vorticity of the idealized solid body. The circulation of the vortex is the

area under this curve.

The situation where a breakdown occurs in a steady vortex is considered to be the superposition of two flow cases. Case I is the condition where all of the velocities in the flow are due to the disturbance. This case I is therefore a large disturbance theory. This case is difficult to realize experimentally due to the requirement of a substantial steady free stream velocity in order to observe correspondingly substantial disturbed state velocities.

From photographic data existing from prior experimentation (Granger, Ref 1) it can be seen that the breakdown has a periodic structure. The velocities and pressures for Case I are assumed to be as follows:

$$v_r = \bar{v}_r(r)e^{ik} \qquad \ldots 5)$$

$$v_\theta = \bar{v}_\theta(r)e^{ik} \qquad \ldots 6)$$

$$v_z = \bar{v}_z(r)e^{ik} \qquad \ldots 7)$$

$$p = \bar{p}(r)e^{ik} \qquad \ldots 8)$$

(14)

where

$$K \equiv \lambda z + \phi + \sigma t \qquad ...9)$$

The amplitudes of the mean velocities $\overline{V_r}$, $\overline{V_\theta}$, and $\overline{V_z}$ are assumed to be dependent on the radius.

Case II would be the physically realizable case where there is no disturbance and the velocities and pressures are independent of time. The undisturbed flow consists of an essentially axial free stream velocity and a rotational velocity. Steady velocities and pressures are given as

$$v_r = 0 \qquad ...10)$$

$$v_\theta = \sum_{n=1}^{\infty} a_n(z) r^{n-1} \qquad ...11)$$

$$v_z = V(r,z) \qquad ...12)$$

$$p = P(r,z) \qquad ...13)$$

The general form for the tangential velocity in eq. 7) is used to fit curves of actual data collected

using the LDV. In the potential vortex, n=0, and $a_n=\Gamma_\infty/2c$.

When a disturbance is present the velocities are assumed to be a simple superposition of Case I and Case II as seen in the following equations:

$$v_r = \bar{v}_r(r)e^{ik} \qquad ...14)$$

$$v_\theta = \sum_{n=1}^{\infty} a_n(z)r^{n-1} + \bar{v}_\theta(z)e^{ik} \qquad ...15)$$

$$v_z = V(r,z) + \bar{v}_z(r)e^{ik} \qquad ...16)$$

$$p = P(r,z) + \bar{p}(r)e^{ik} \qquad ...17)$$

The boundary layer thickness is determined by the relationship between the velocities defined as

$$v_\theta(z) = V_\infty\left(1 - e^{-q(z)^n}\right) \qquad ...18)$$

The boundary layer thickness is defined as the z location where the velocity is 99% of V_∞.

Eulers equations of motion in component

cylindrical form are

$$\text{radial: } \frac{\partial v_r}{\partial t} + v_r \frac{\partial v_r}{\partial r} + \frac{v_\theta}{r} \frac{\partial v_r}{\partial \theta} - \frac{v_\theta^2}{r} + v_z \frac{\partial v_z}{\partial z} = \frac{-1}{\rho} \frac{\partial p}{\partial r} \qquad \ldots 19)$$

$$\text{rotational: } \frac{\partial v_\theta}{\partial t} + v_r \frac{\partial v_r}{\partial r} + \frac{v_\theta}{r} \frac{\partial v_\theta}{\partial \theta} + \frac{v_r v_\theta}{r} + v_z \frac{\partial v_\theta}{\partial z} = \frac{-1}{\rho} \frac{\partial p}{r \partial \theta} \qquad \ldots 20)$$

$$\text{axial: } \frac{\partial v_z}{\partial t} + v_r \frac{\partial v_r}{\partial r} + \frac{v_\theta}{r} \frac{\partial v_r}{\partial \theta} + v_z \frac{\partial v_z}{\partial z} = \frac{-1}{\rho} \frac{\partial p}{\partial z} \qquad \ldots 21)$$

Substituting the assumed solution of eqs. 14) - 17) into eqs. 19) - 21) yields the following:

$$\text{radial: } i\sigma \bar{v}_r + \left[\bar{v}_r \frac{\partial \bar{v}_r}{\partial r} + i \frac{\bar{v}_\theta \bar{v}_r}{r} - \frac{\bar{v}_\theta^2}{r} + i\lambda \bar{v}_z \bar{v}_r \right] e^{ik} = \frac{-1}{\rho} \frac{\partial \bar{p}}{\partial r} \qquad \ldots 22)$$

$$\text{rotational: } i\sigma \bar{v}_\theta + \left[\bar{v}_r \frac{\partial \bar{v}_\theta}{\partial r} + i \frac{\bar{v}_\theta^2}{r} + \frac{\bar{v}_r \bar{v}_\theta}{r} + i\lambda \bar{v}_z \bar{v}_\theta \right] e^{ik} = \frac{-i}{\rho} \frac{\bar{p}}{r} \qquad \ldots 23)$$

$$\text{axial: } i\sigma \bar{v}_z + \left[\bar{v}_r \frac{\partial \bar{v}_z}{\partial r} + i \frac{\bar{v}_z \bar{v}_\theta}{r} + i\lambda \bar{v}_z^2 \right] e^{ik} = \frac{-i\lambda}{\rho} \bar{p} \qquad \ldots 24)$$

The pressure terms in eqs. 22) - 24) are eliminated by multiplying the terms in eq. 22) by the imaginary constant ($-i\lambda$) and adding the results of

that multiplication to the partial derivative with respect to the radius r of the terms in the axial eq. 24). The result is as follows:

$$\lambda\sigma\bar{v}_r + i\sigma\frac{\partial\bar{v}_z}{\partial r} + \left[\lambda\frac{\bar{v}_\theta\bar{v}_r}{r} - i\lambda\bar{v}_r\frac{\partial\bar{v}_r}{\partial r} + \lambda^2\bar{v}_z\bar{v}_r + \frac{i\lambda\bar{v}_\theta^2}{r} + \frac{\partial\bar{v}_r}{\partial r}\frac{\partial\bar{v}_z}{\partial r} + \bar{v}_r\frac{\partial^2\bar{v}_z}{\partial r^2} - i\frac{\bar{v}_z\bar{v}_\theta}{r^2} + i\frac{\bar{v}_\theta}{r}\frac{\bar{v}_z}{\partial r} + i\frac{\bar{v}_z}{r}\frac{\partial\bar{v}_\theta}{\partial r} + 2i\lambda\bar{v}_z\frac{\partial\bar{v}_z}{\partial r}\right]e^{ik} = 0 \qquad \ldots 25)$$

Next we multiply the terms in the axial equation by 1/r and subtract the terms in the axial equation from λ multiplied by the terms in the rotational equation. The result is as follows:

$$i\lambda\sigma\bar{v}_\theta - i\sigma\frac{\bar{v}_z}{r} + \left[\lambda\bar{v}_r\frac{\partial\bar{v}_\theta}{\partial r} + i\lambda\frac{v_\theta^2}{r} + \lambda\frac{\bar{v}_r\bar{v}_\theta}{r} + i\lambda^2\bar{v}_z\bar{v}_\theta - \frac{\bar{v}_r}{r}\frac{\partial\bar{v}_z}{\partial r} - \frac{i\bar{v}_z\bar{v}_\theta}{r^2} - i\lambda\frac{\bar{v}_z^2}{r}\right]e^{ik} = 0 \qquad \ldots 26)$$

Certain terms appearing in eqs. 25) and 26) can be eliminated by subtracting eq. 26) from eq. 25) to yield the complex equation,

$$\lambda\sigma(\bar{v}_r - i\bar{v}_\theta) + i\sigma\left(\frac{\partial}{\partial r} + \frac{1}{r}\right)\bar{v}_z + \left[-\lambda\left(\bar{v}_r\frac{\partial\bar{v}_\theta}{\partial r} + i\bar{v}_r\frac{\partial\bar{v}_r}{\partial r} + \frac{\partial v_z}{\partial r}\left(\frac{\partial}{\partial r} + \frac{1}{r}\right)\bar{v}_r + \right.\right. \quad (18)\ldots 27)$$
$$\left.\left.\lambda^2\bar{v}_z(\bar{v}_r - i\bar{v}_\theta) + \frac{i}{r}\bar{v}_\theta\frac{\partial\bar{v}_z}{\partial r} + i\lambda\left(\frac{\partial}{\partial r} + \frac{1}{r}\right)v_z^2 + \bar{v}_r\frac{\partial^2 v_z}{\partial r^2} + \frac{i}{r}\bar{v}_z\frac{\partial v_\theta}{\partial r}\right]e^{ik} = 0$$

Substituting the continuity equation

$$\left(\frac{\partial}{\partial r} + \frac{1}{r}\right)\bar{v}_r = -i\left(\frac{\bar{v}_\theta}{r} + \lambda\bar{v}_z\right) \qquad \ldots 28)$$

into eq. 27) and multiplying through by e^{-ik} yields

$$\left[\lambda\sigma(\bar{v}_r - i\bar{v}_\theta) + i\sigma\left(\frac{\partial}{\partial r} + \frac{1}{r}\right)\bar{v}_z\right]e^{-ik} - \lambda\left(\bar{v}_r\frac{\partial\bar{v}_\theta}{\partial r} + i\bar{v}_r\frac{\partial\bar{v}_r}{\partial r}\right) -$$
$$i\lambda\bar{v}_z\frac{\partial\bar{v}_z}{\partial r} + \lambda^2\bar{v}_z(\bar{v}_r - i\bar{v}_\theta) + i\lambda\left(\frac{\partial}{\partial r} + \frac{1}{r}\right)\bar{v}_z^2 + \bar{v}_r\frac{\partial^2\bar{v}_z}{\partial r^2} +$$
$$\frac{i}{r}\bar{v}_z\frac{\partial\bar{v}_\theta}{\partial r} = 0 \qquad \ldots 29)$$

Equation 29) is applicable in the flow region from the condition upstream as well as downstream from the breakdown structure. In the breakdown region, the flow is unsteady. There is a prominent circular frequency associated with the decay, but the point where the decay transpires is variable. The result is a standing wave behind the breakdown region of a particular wave length.

For this case, we define

$$\sigma = 0 \qquad \text{...30)}$$

to represent the flow upstream of the breakdown phenomenon.

Applying eq. 30) to eq. 29), the bracketed term falls out. The remaining equation is separated into real and imaginary parts yielding the following:

$$\text{Real: } \frac{\partial^2 \bar{v}_z}{\partial r^2} + \lambda^2 \bar{v}_z = \lambda f(r) \qquad \text{...31)}$$

$$\text{Imaginary: } -\lambda \bar{v}_r \frac{d\bar{v}_r}{dr} - \lambda \bar{v}_r \frac{d\bar{v}_z}{dr} - \lambda^2 \bar{v}_z \bar{v}_\theta + \lambda \left(\frac{d}{dr} + \frac{1}{r}\right) \bar{v}_z^2 + \frac{1}{r} \bar{v}_z \frac{d\bar{v}_z}{dr} = 0 \qquad \text{...32)}$$

when

$$f(r) = d\bar{v}_\theta / dr \qquad \text{...33)}$$

Equation 31) is applicable for the general case where the breakdown is not required to be axisymmetric. The partial derivative with respect to θ is not required to be zero for this solution due to the inclusion of the azimuthal variation term in eq.

9).

Equations 31) and 32) describe the flow according to the discussed assumptions derived from observations. The boundary conditions for these equations in the steady flow where eq. 30) is satisfied are as follows:

a) At $z=0$, $0 \leq r \leq r_c$ (where r_c is the radius of the core), the tangential velocity, V_θ, is given by

$$\overline{v}_\theta = \omega r \qquad \ldots 34)$$

which is valid for solid body rotation when angular velocity, v_θ, is constant.

b) Experimental observation indicates that as z increases for $0 \leq r \leq r_c$, the tangential velocity, V_θ decreases in magnitude. Thus eq. 34) is modified to

$$\overline{v}_\theta = \omega r (1 - e^{-r/z}) \qquad \ldots 35)$$

for $0 \leq r \leq r_c$.

The flow described by eq. 29) includes the

backwash region trailing the breakdown as the formation moves up the centerline of the vortex. Equation 29) establishes the theory that can be used to support measurements of the core radius and circulation in this region.

If measurements of circulation and the core radius could be made before and after the breakdown formation and those measurements were put into the proper non-dimensional format, the flow would be found to exhibit supercriticality before the breakdown and subcriticality afterwards. It is possible that the proper non-dimensional format would be similar to the format of the Froude number, Fr, for open channel flow. In this way, the Froude number could be defined for vortex flows as

$$F_{rot} = \frac{\Gamma}{r_c^{3/2}\sqrt{g}} \qquad \ldots 36)$$

If this number is found to be greater than unity before the breakdown, and less than unity after the breakdown, the phenomenon of vortex breakdown would appear to be a critical flow situation with a criticality defined by eq. 36)

EXPERIMENTAL PROCEDURE

Step 1) Facility

The vortex generator in Figure 2 of Appendix A was built with a flat window 16cm wide running the height of the cylinder. The window was required to allow laser Doppler velocimetry (LDV) measurements. If the LDV beams pass through a curved interface where two materials of different indices of refraction meet, the surface will act as a lens. The LDV cannot be calibrated to take this additional focusing effect into account for more than one radial location. Since this experiment investigates a multitude of radial locations, a flat interface is required.

The vortex generator is used in this application to create a vortex with a water column depth of 46 inches and a sink radius of .25 inches.

Step 2) Instrumentation

The LDV optical instrumentation was set up as shown in Figures 7, 8, & 9. Figure 7 shows the transmitting optics schematic. Figure 8 shows the

receiving optics schematic. Figure 9 is a legend that applies to Figures 7 and 8. A more detailed discussion of the setup and alignment of the optical instrumentation can be found in Appendix D.

Step 3) Calibration

A spinning disc of known radius and known radial velocity was used to align the LDV and determine the fringe spacing. A more detailed discussion of calibration of LDV instrumentation can be found in Appendix D. Calculations concerning this calibration can be found in Sample Calculations.

Step 4) Quantitative Data Collection

a) LDV instrumentation was used to take measurements of axial and tangential velocities from a radius of -10mm, through the core of the vortex, and out to a radius of 210mm. This set of measurements was taken at a variety of axial locations and a variety of valve settings.

b) Tangential velocity data were used to determine ambient circulation for a given valve setting using

the following

$$\Gamma = 2\pi r V_\theta \qquad \ldots 37)$$

After the ambient circulation for a given valve setting was determined, data taken at that valve setting are referenced by this circulation.

c) For three different circulations, LDV was utilized to produce tangential velocity data at twelve radial locations ranging from r=10mm out to r=175mm from a height of 50mm above the bottom of the cylinder down to as close to the bottom as the apparatus would allow. A limit was found to exist on the height that the LDV would measure at the low radial locations. The cause of this limit is explained in the Discussion of Results.

d) Axial velocities were determined using the LDV for all stations investigated in item c).

Step 5) Qualitative Observation

a) Food coloring was injected into the bottom

boundary layer near the inner vertical cylinder in order to obtain qualitative observations of dominant velocities throughout the boundary layer.

b) Dichlorofluorescein was injected just beneath the free surface outside of the core as well as on the centerline. This allowed qualitative observations of the flow situation in and around the core of the vortex, as well as the mechanism for the feeding of vorticity to the core.

c) A glass rod was placed in front of the multicolor beam of the laser. This split the beam into a two dimensional sheet of laser light. Photographs were made of the laser sheet intersecting the vortex at various angles including a vertical intersection of the vortex core in the region of the sink.

RESULTS

The graphical results of items 1 through 7 are shown in Appendix B.

1) Circulation, Γ, was determined from the tangential velocities at the given radial locations using eq. 37). Circulation was plotted vs. radius for three different valve positions. The radial distribution of circulation for three different values is presented in Graph 2.

2) Graph 3 shows the distribution of tangential velocity for three different circulations. Plots were made from data taken at a distance of 50mm from the plate. Positive tangential velocities are left to right perpindicular to the axis of the LDV beams.

3) Radial profiles of axial velocity for the above circulations are in Graph 4. Positive axial velocities are shown as being downward.

4) Core radius was plotted for three different circulations in Graph 5.

5) General trends for other flow situations observed were that higher axial locations resulted in less accuracy of the beam alignment to the actual center of the vortex, lower axial locations resulted in loss of data rate and corresponding drop in accuracy due to a lower number of values being averaged per point. Higher axial locations resulted in larger core radii and smaller maximum velocities.

6) The radial distributions of vorticity for the three different circulations are plotted in Graph 6.

7) The axial variation of tangential velocity, V_θ, are plotted in Graphs 7-11. These plots were useful in determining the thickness of the boundary layer.

8) Flow visualization showed the tangential velocity

to be dominant on the outermost edges of the base. However, a significant radial velocity carried the flow inwards along the boundary layer. As radius decreased, the magnitude of the radial velocity in the boundary layer increased, until near the sink the radial velocity was the most dominant.

9) A photograph of the injection technique and results near the free surface is Figure 5 of Appendix A. The dichlorofluorescein was injected with a hypodermic needle placed just beneath the free surface tangential to the flow. This flow visualization shows that the dominant velocity outside of the core away from the boundary layer is tangential velocity. A radial velocity does exist. The flow inside the core is dominated by a downward axial velocity.

10) The creation of a 2 dimensional sheet of laser light coupled with the use of fluorescent dye allowed the experimenter to observe all three velocity components. A typical photograph is shown in Figure 10 of Appendix A. Specific

pertinent observations are discussed in the Discussion of Results section of this report.

DISCUSSION OF RESULTS

1) Circulations were calculated after the data were taken. Higher circulations correspond to higher flow rates as per Granger ref. 1 (eq. 55 on pg 73). In the irrotational region of the vortex, circulation is relatively constant. Circulation is proportional to both V_θ and radius as shown by eq. 37). There is a range of radial locations in Graph 2 where the curve for a circulation of 171 cm^2/s is actually above the curve for 188 cm^2/s. This could be due to the time variance of the centerline location of the vortex. However, the average over the radius well outside of the core radius corresponds to the determined value of circulation.

2) The plots of tangential velocity vs. radius (Graph 3) show a region outside of the core where the tangential velocity is inversely proportional to the radius. This corresponds to the theoretical zero vorticity in the region outside of the core.

At the core radius, the tangential velocity is a maximum. Across the core the tangential velocity vs. radius curve is almost linear. A linear tangential velocity profile corresponds to the solid body rotation idealization. The plot of tangential velocity vs. radius for a solid body has a constant vorticity and therefore a linear tangential velocity vs. radius plot. The vorticity measured in this application was found to be dependent on radius. Therefore, this vortex does not exhibit true solid body rotation and so the tangential velocity profile across the core radius is not precisely linear.

Therefore, this plot shows that a substantial vorticity exists in the core region compared to a negligible vorticity in the region outside of the core. This leads to the question of how the vorticity is fed into the core region from the tangential influx in the near irrotational region.

3) The axial velocity profiles in Graph 4 show a region of substantial updraft just outside of the core and agrees with Granger's observations in ref

1. A photograph which depicts this updraft is Figure 11 in Appendix A. Figure 11 shows an injection of dye at a low axial location and the subsequent transport of that dye to higher axial locations. This is surprising due to the close proximity of an enormous axial velocity in the opposite direction down the centerline. This photograph shows the approximate size of the streamtube on an approximate 1:1 scale.

If there exists a cell with an axial updraft around the core as these data indicate, then no flow can pass the cell except through diffusion, and vorticity feeding cannot occur anywhere above a given axial location.

This would indicate that the flow and subsequent vorticity feed is entering the core through some feeding mechanism that is at a low axial location (i.e. the boundary layer). Therefore, a description of the flow situation near the core in the boundary layer is desirable.

4) In Graph 5, the lower mass flow rates correspond to larger core radii. This agrees with Granger's

findings in Ref 1 & 2. This is one of the variables desired for the determination of a non-dimensional parameter that describes the vortex breakdown.

5) The core spreading with higher axial location agrees with Granger's observations in Ref 1 & 2.

6) The vorticity vs. radius plots (Graph 6) deviate from the theoretical results described in Graph 1. The deviation is in that the middle circulation seems to have a higher vorticity than the largest circulation, and a larger core radius than the lowest circulation. The possible source of error in this deviation is the same as in the deviation of the circulation of the middle valve setting in item 1). The two higher circulations were actually so close that meaningful comparisons can only be made between either of the higher two and the smallest one. Since circulation is the area under the vorticity curve, if the higher circulation has a lower core radius, then the

maximum vorticity must be very high in order to result in a higher overall area.

7) None of the graphs of boundary layer velocities (Graphs 7 - 11) continue to the plate (z=0). The measurements taken at relatively large radii were able to obtain significant data only down to an axial location of 5 mm above the plate. As the measurement volume descended closer and closer to the plate, the signal strength of the scattered light dropped off until it was lost in the ambient noise. It was easier to collect data at low axial locations for two reasons: 1) The returning signal had to travel through less water to return, (the seeded water is cloudy and attenuates the signal much more so than air,) and 2), the amount of scattered light actually blocked by the plate is less at the larger radii.

The limit of axial proximity to the plate is 5mm due to the glue on the base of the 16 cm window that is required to keep watertight integrity. At axial locations below 5mm, parts of the beams are actually passing through the glue.

Therefore, no return signal will be received.

8) These observations show that the radial velocity in the boundary layer increases with decreasing radius as far as the sink radius. As the radius decreases, the proportion of radial velocity to the tangential velocity increases. In other words, the flow goes from a situation dominated by tangential velocities at large radii to a situation dominated by radial velocity at small radii until the flow reaches the sink radius. At the sink radius, the radial flow follows the turn and goes down into the sink. Then the flow is reversed and comes out of the sink and into the axial updraft region surrounding the core.

9) The photograph in Figure 5 of Appendix A illustrates that this vortex is a three dimensional one. There is a pronounced tangential velocity as evidenced by the swirling flow. A radial velocity is present as evidenced by the spiral in towards the center. An axial velocity is dominant in the core as evidenced by the

centerline marking by the dye in the middle of the vortex.

10) The flow visualization has exposed the flow trends in and around the core near the boundary layer. The flow in this region is extremely complicated. Observations show that there is the expected maximum downward axial velocity in the center. Directly adjacent and within the sink radius is a substantial reversal of flow. The dye pathlines indicate that the fluid and vorticity feeding from the surface and outer influx into the core and subsequently down the sink is accomplished as follows: The particle travels down the confined bell-shaped region that surrounds the core. When the outer bell-shaped region of downward axial velocity reaches the boundary layer, the fluid particles follow a path just along the top of the boundary layer and enter the outer portion of the sink hole. Somewhere inside the sink, the flow separates and spurts out of the sink hole to form the region of the updraft quantified in Graph 5 in Appendix B.

This technique has produced a determination of the flow situation in the region where the viscous core region, the viscous boundary layer, and the near irrotational region of the vortex meet and interact. This is the critical region of importance because this is the region where the vortex breakdown structure initially forms with an obstruction in the flow, and this is the region where many of the simplifying assumptions do not hold true.

CONCLUSIONS

1) There is an inverse relationship between the core radius and the ambient circulation of a vortex shown on Graph 5.

2) The flow visualization technique utilizing a two dimensional sheet of laser light and dichlorofluorescein injected just beneath the free surface is extremely effective in this application.

3) The complicated area in the region near the sink where the formation of the vortex breakdown initially occurs consists of the location where three simpler regions meet: The near irrotational region, the viscous core, and the viscous boundary layer.

4) The axial flow situation in the region near the sink consists of high downward axial velocities at the centerline that decrease in magnitude

parabolically out to the core radius. Some distance outside of the core radius the flow reverses and there is a region of high upward axial velocities. At the sink orifice, there is one more reversal of flow before reaching the sink radius. This is the flow that feeds the updraft. The flow travels from the boundary layer into the outer radii of the sink, reverses into the updraft region, and eventually feeds into the core along the axial extent.

5) The tangential velocity situation in the region near the sink consists of highly rotational flow within the vortex core, near irrotational flow well outside of the core, and a less intense rotational flow in the region of the updraft. Vorticity seems to be fed from the outside of the vortex into the outer shell of downward axial velocity, down to the boundary layer, radially inward towards the sink, into the sink to some depth, back out in the updraft region, and then into the vortex core along the axial extent of the vortex.

6) The radial velocity situation in the region near the sink consists of increasing radial velocity along and within the boundary layer as a fluid particle travels inward toward the sink. This increasing radial velocity is a result of the radial boundary layer flow feeding the updraft region around the core. The updraft is fed by a steady flow. If that flow originates from a radial flow in the boundary layer, then the radial flow would exhibit an increasing velocity with decreasing radius until it reaches the sink. When it does reach the sink, the radial flow is redirected in the axial direction down the sink, and then through a flow reversal and upwards in the axial updraft region.

7) Since actual numerical data could not be taken in the region of the sink, this investigation could not be used to support or refute any theories of the mechanism of vortex breakdown. However, it has shed light on measurement techniques, possible ways to approach the problem, and it was able to qualitatively expose the flow situation in the

critical region of the instigation of the vortex breakdown formation.

RECOMMENDATIONS

1) Determine an expression for core radius as a function of circulation by running a large number of tangential velocity profiles under many different valve settings and subsequent circulations.

2) Investigate new LDV system setup ideas that could provide data in the center near the bottom plate.

3) Align LDV system so that radial velocity profiles are possible. This can be done by traversing the present setup in the X direction instead of the Y direction. Y must remain zero. However, more alignment and experimentation must be done before radial velocities will be meaningful.

4) Use the two-dimensional laser sheet flow visualization technique in conjunction with high resolution video or high speed photography and a local reference for scale in order to quantify the

flow situation around the core-boundary layer interaction region.

5) Modify the sink orifice so that dye can be injected at different depths. This will indicate how far down the flow reversal region goes inside the sink.

6) Perform measurements on the transient phenomenon to determine the values of core radius, vorticity, and circulation before and after the breakdown passes through a point. This would require software that can give a time history of LDV measurements (such as the TSI Intelligent Flow Analyzer 550) which are not owned by the USNA.

REFERENCES

1) Granger, R.A., "A Steady Axisymmetric Vortex Flow", Geophysical Fluid Dynamics, 1972, Vol. 3, pp45-88.

2) Granger, R.A., "Steady Three-Dimensional Vortex Flow", Journal of Fluid Mechanics, 1966, Vol. 25, part 3, pp 557-576.

Other Reading

Oser, Hansjörg, "Erzwungene Schwingungen in Rotierenden Flüssigkeiten", Archive for Rational Mechanics and Analysis, Vol. 1, No. 1, 1957, P. 81-96.

Thomson, Sir William, "Vibrations of a Columnar Vortex", Mathematical & Physical Papers, Cambridge University Press, 1910, pp 162-165.

SAMPLE CALCULATIONS

Calibration of Fringe Spacing

Blue Tang	wheel speed	+1.2 rps
	freq (Mhz)	.084325
Blue Vert		.6 rps
		.03306

.6 rps @ 2.5 cm radius ⇒ 9.425 cm/s

1.2 rps @ 2.5 cm radius ⇒ 18.85 cm/s

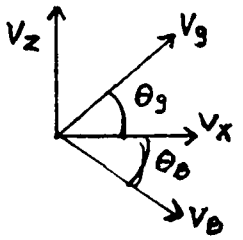

$(f_B - .05) \times d_B = V_B = V_x \cos\theta_B - V_z \cos(90 - \theta_B)$

(shift)

$= V_x \cos\theta_B - V_z(\sin\theta_B)$

Blue vert $[.03306 - .05] d_B = -.09425 \sin\theta_B \quad d_B = \frac{-.09425}{-.01694} \sin\theta_B$

$d_B = \sin\theta_B \times 5.56375$

Blue tang $[.084325 - .05] d_B = .18850 \cos\theta_B \quad d_B = \frac{.18850}{.034325} \cos\theta_B$

$d_B = 5.492 \cos\theta_B$

$$\frac{\sin\theta_B}{\cos\theta_B} = \frac{5.492}{5.564} = \tan\theta_B$$

Resolution of Components

given $\theta_G = 48.69°$ $\quad V_B = V_x .7133728 - V_z .7007848$

$\theta_B = 44.49°$ $\quad 1.426972\, V_B = 1.017963\, V_x - V_z$

$V_g = V_x .6601328 + V_z .7511489$

$1.331294\, V_g = .8788308\, V_x + V_z$

$1.8967935\, V_x = 1.426972 V_B + 1.331294 V_g$

$V_x = .752305\, V_B + .7018655\, V_g$

$V_z = .661151\, V_B - .7144729\, V_g$

Circulation Calculation

$\Gamma = 2\pi r V_\theta$ $\quad$ given $V_\theta = 2.011$ cm/s, $r = 100$ mm

$\Gamma = 2\pi\ 10\text{ cm}\ 2.011\text{ cm/s} = 126.3\ \text{cm}^2/\text{s}$

APPENDIX A (figures)

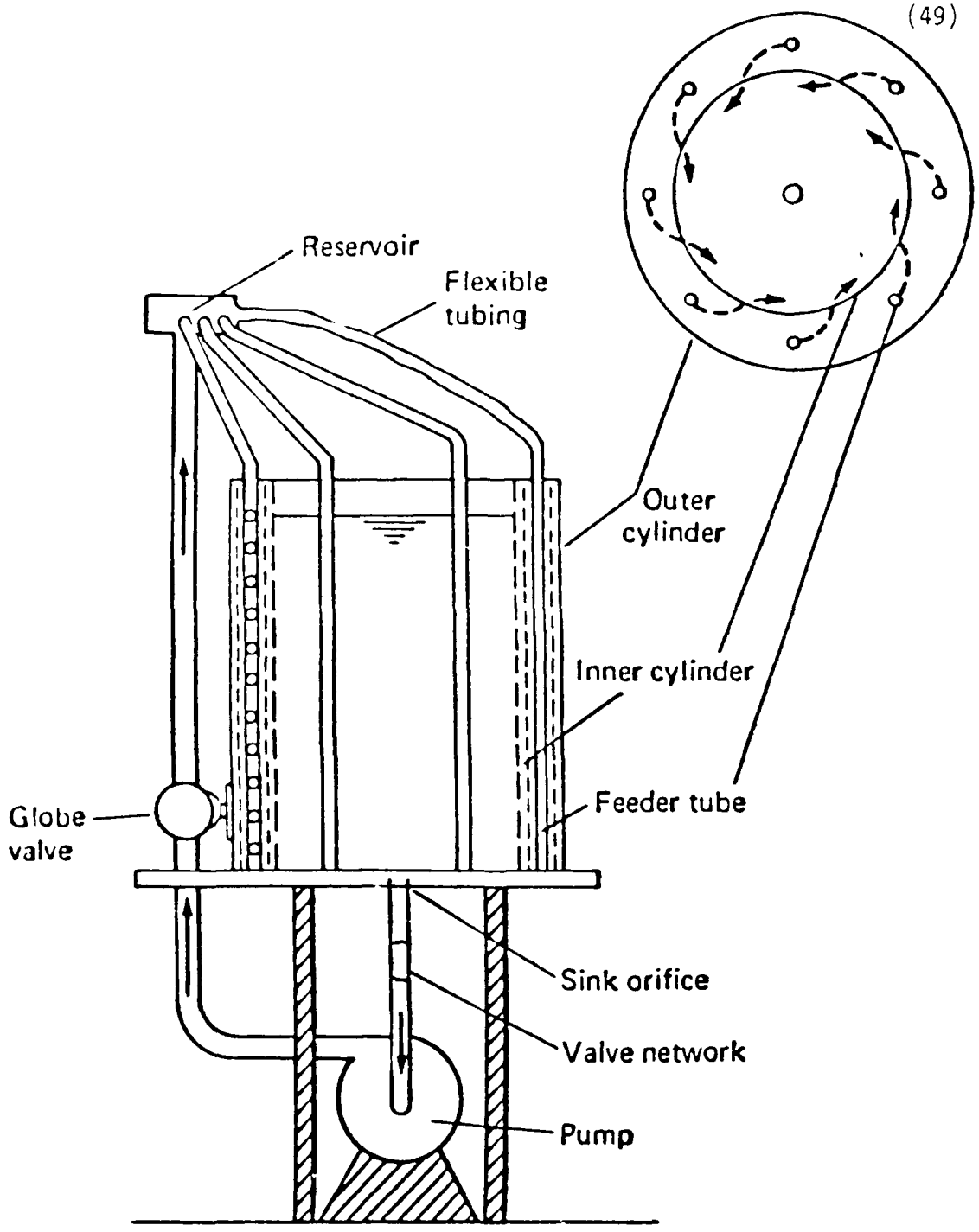
Reservoir
Flexible tubing
Outer cylinder
Inner cylinder
Feeder tube
Globe valve
Sink orifice
Valve network
Pump

figure 2

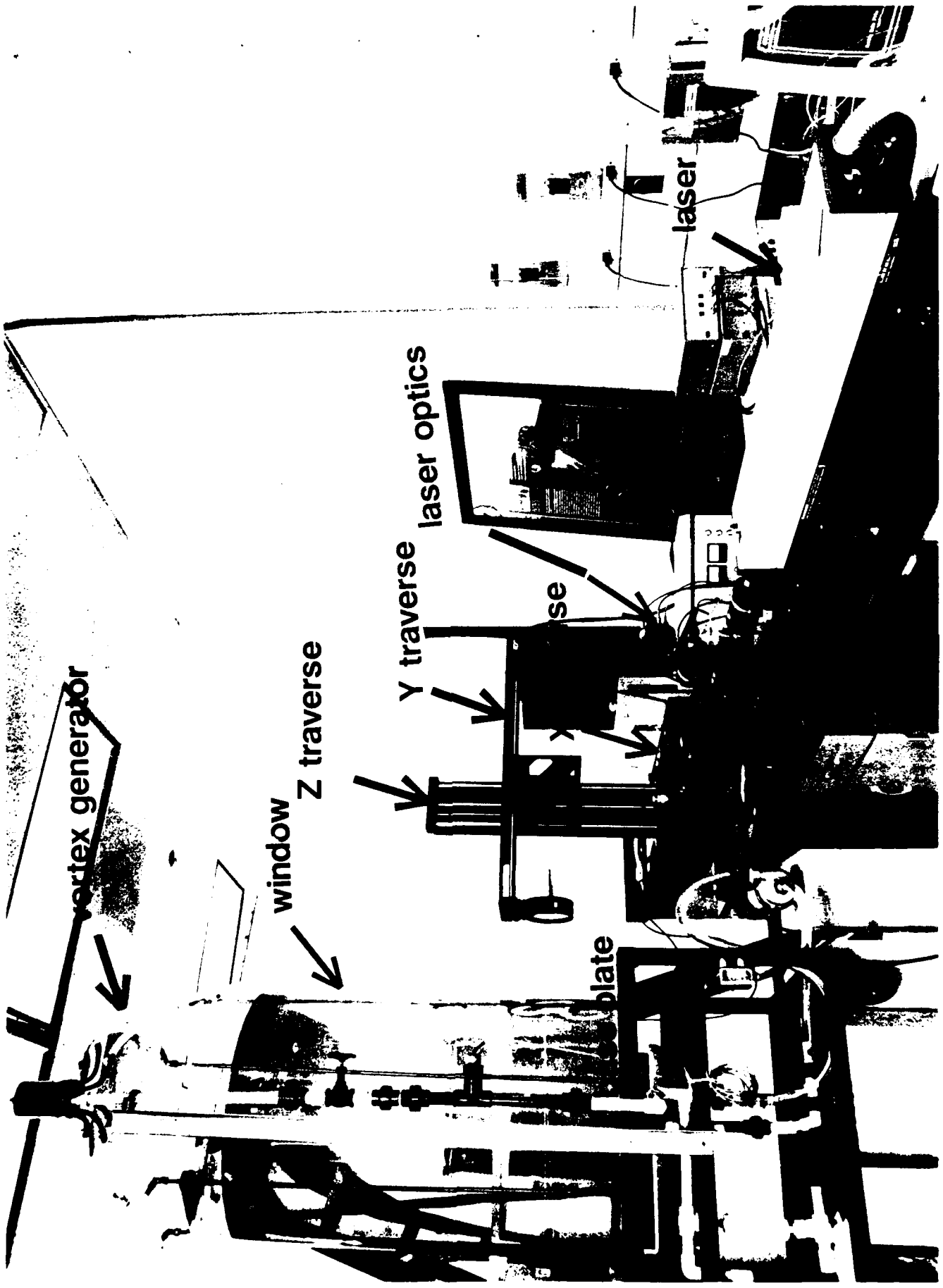
vortex generator
window
Z traverse
Y traverse
laser optics
laser

figure 3

figure 4

Critical Phenomenon

Hydraulic Jump

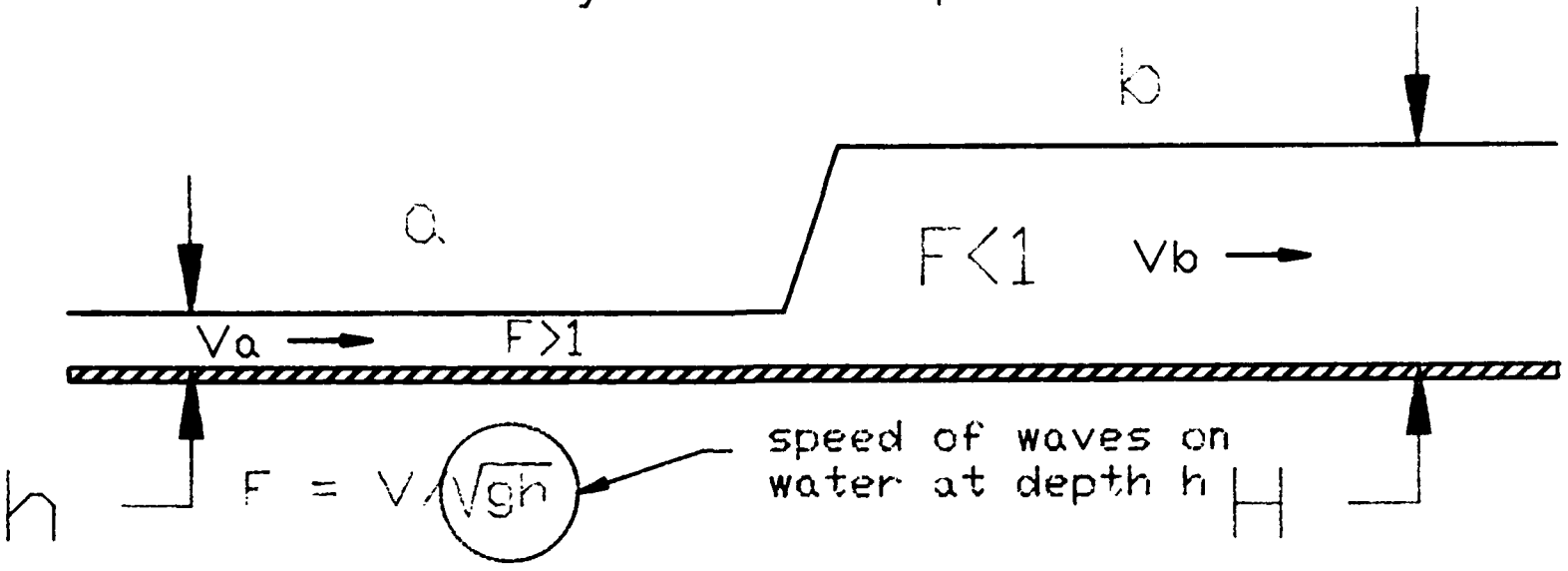

Fa < 1 : flow is subcritical - no jump
Fa > 1 : flow is supercritical

figure 5

Critical Phenomenon

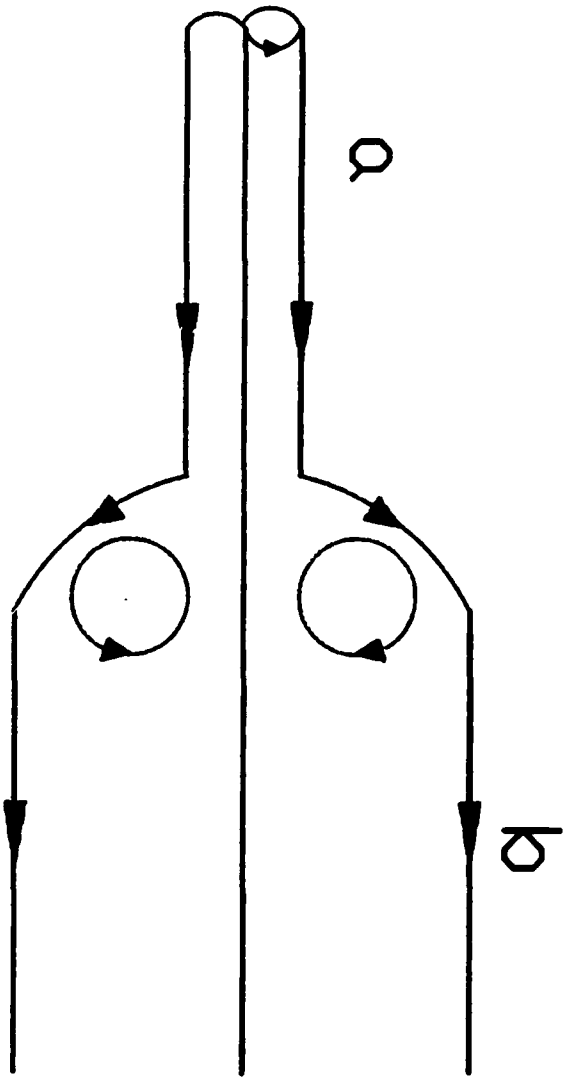

Translational plus rotational flow yields
'equivalent' hydraulic jump?

figure 6

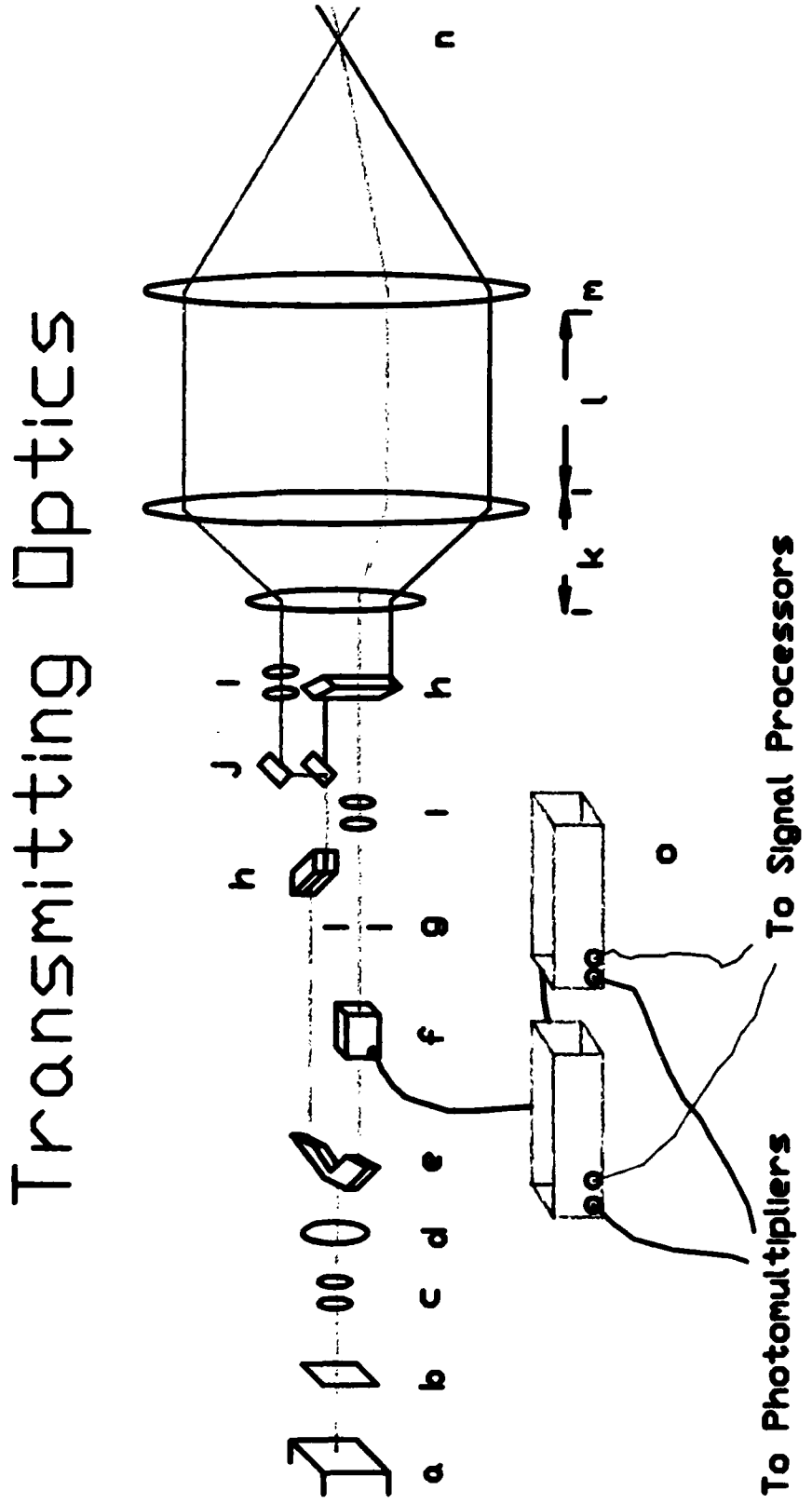
Transmitting Optics
n
m
l
k
j
h
h
g
f
o
e
d
c
b
a
To Signal Processors
To Photomultipliers

figure 7

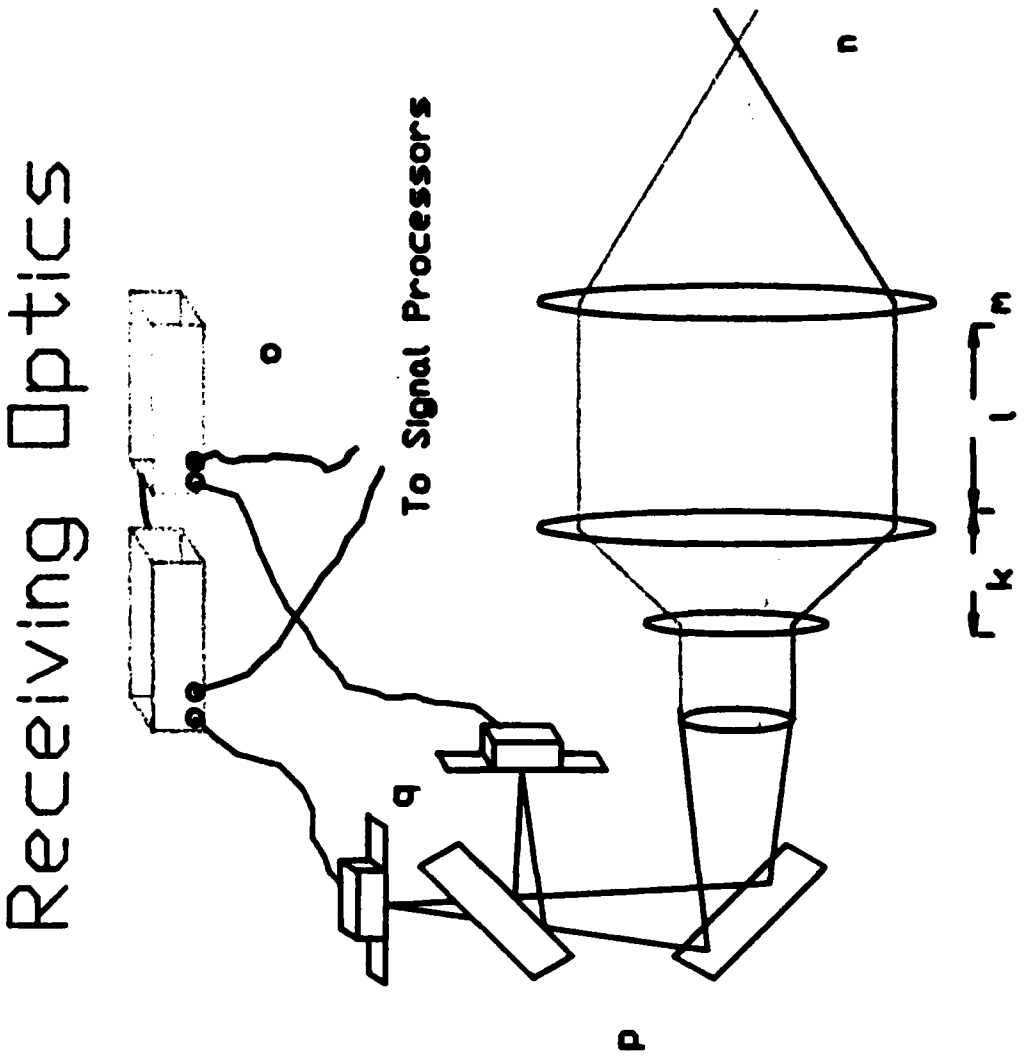

figure 8

Instrumentation Legend

a) Laser orifice
b) Safety Interlock Shutter
c) Beam Collimator
d) Polarization Rotator
e) Beam Splitter
f) Acousto-Optic Modulator
g) Beam Stop
h) Beam Displacer
i) Beam Steering Module
j) Color Separation mirrors
k) Beam Expander
l) Traversing Table
m) Focusing Lens
n) Measurement Volume
o) Frequency Shifters
p) Color Separation Mirrors
q) Photomultiplier Tubes

figure 9

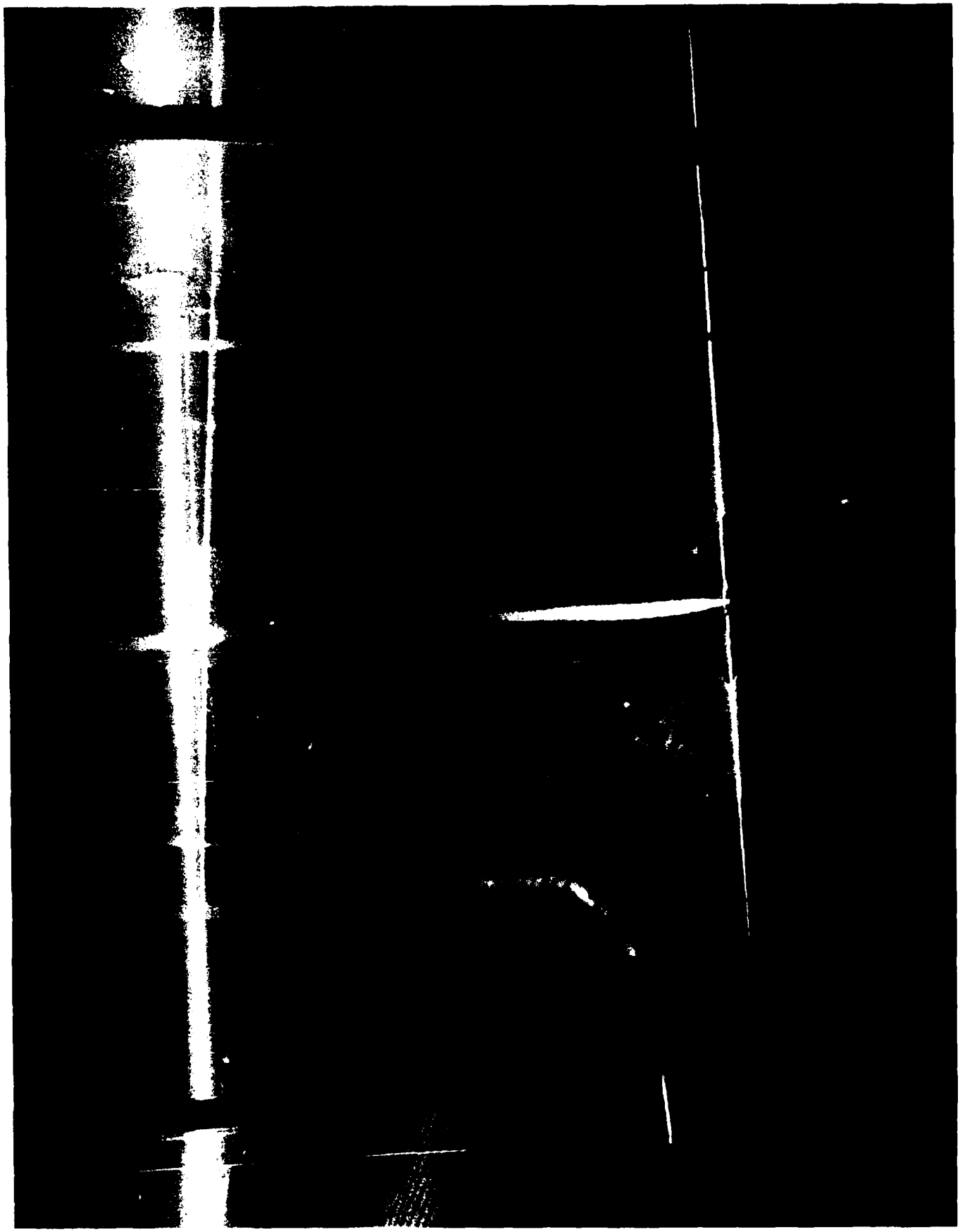

figure 10

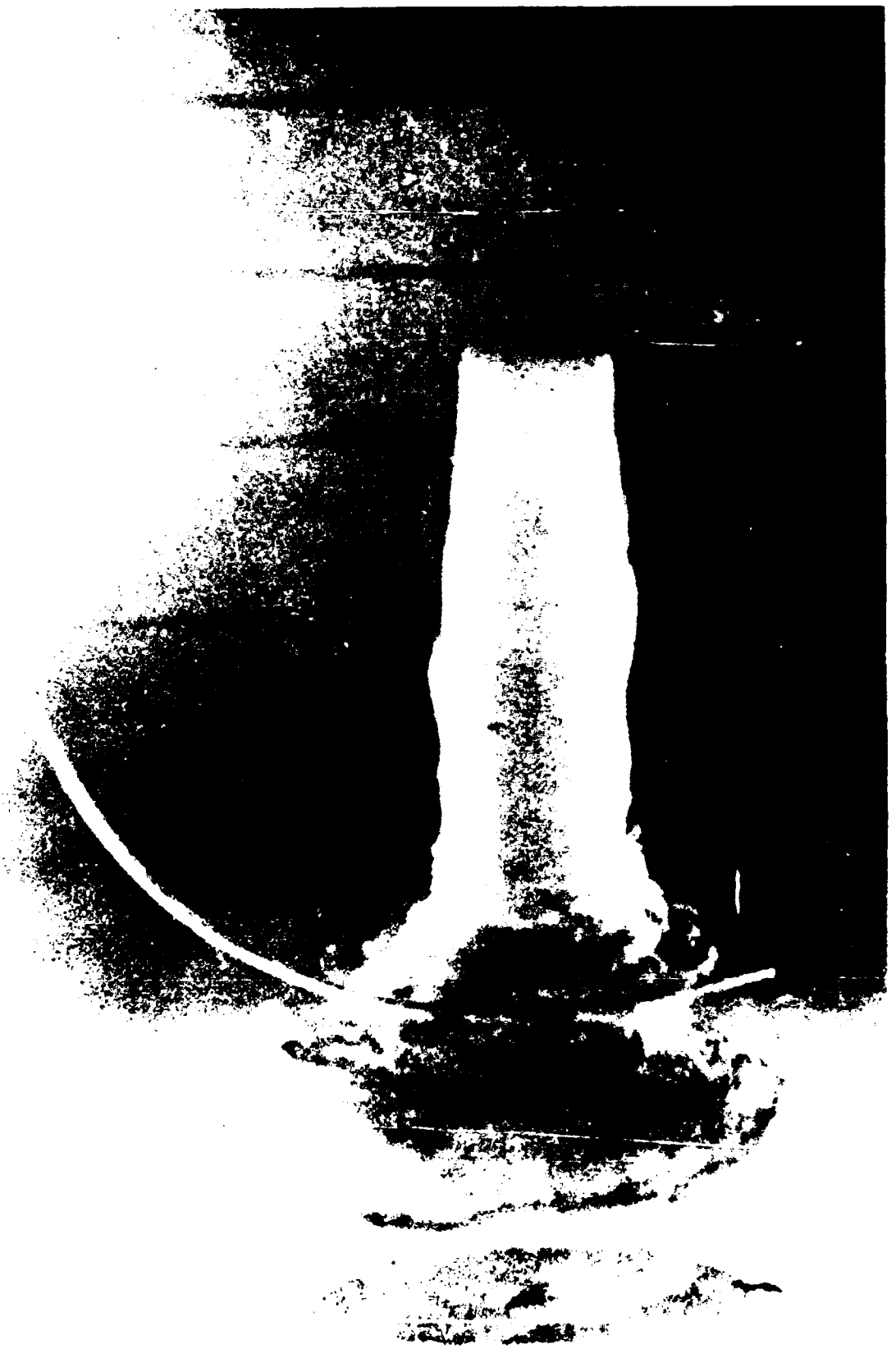

figure 11

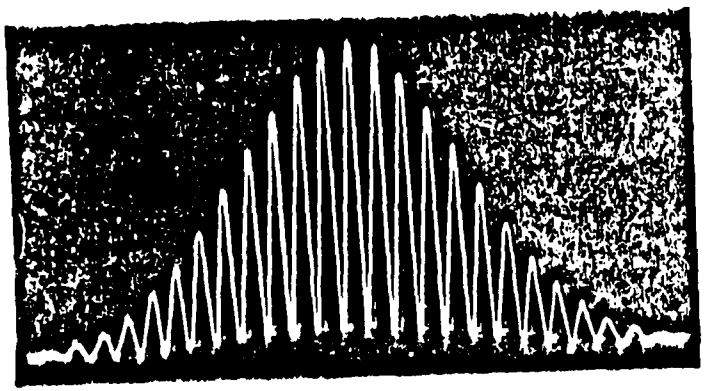

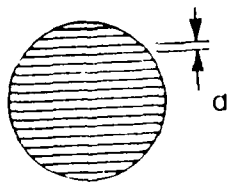

$$d_f = \frac{\lambda}{2 \sin \kappa}$$

$$u_x = f_D d_f$$

Fringe Pattern at Beam Crossing Point

λ = wavelength of incident light

f_D = frequency detected at photodetector

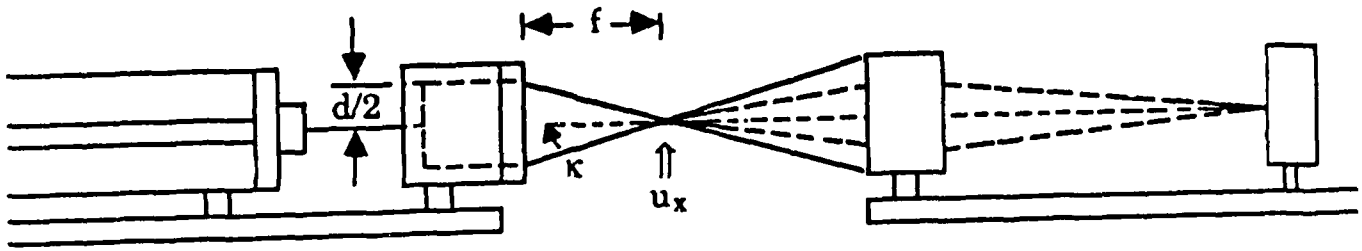

figure 12

APPENDIX B (graphs)

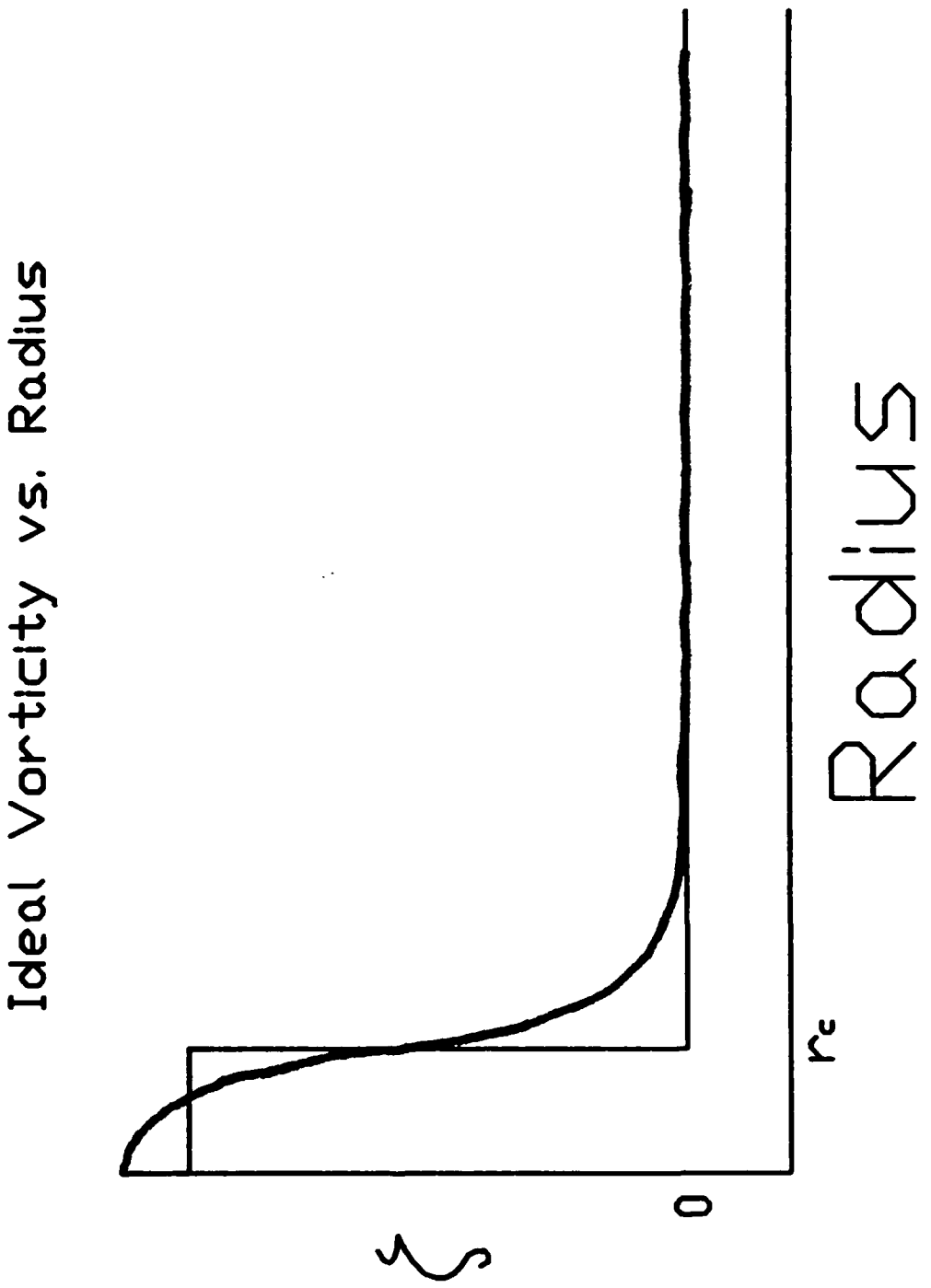

graph 1

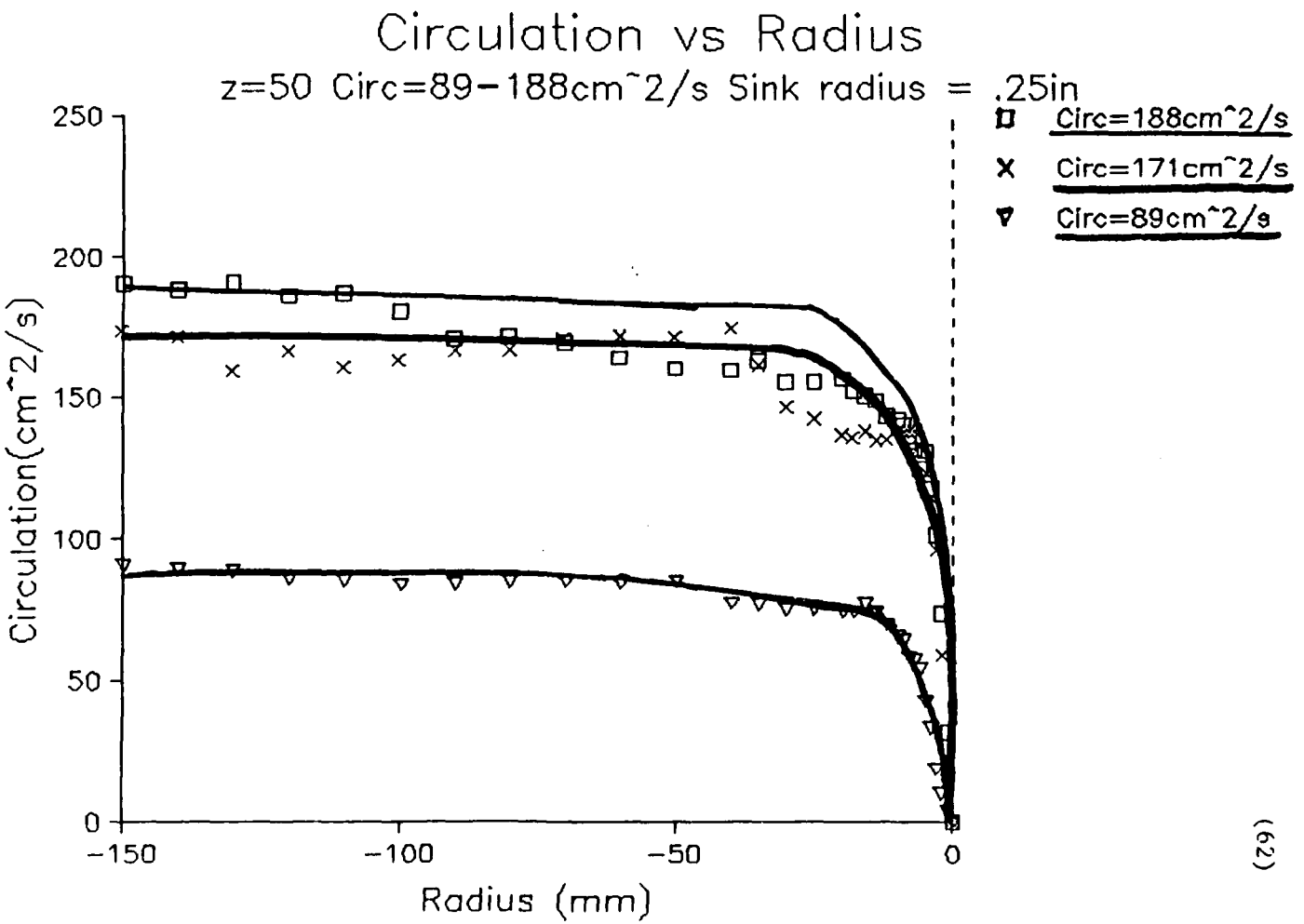
Circulation vs Radius
z=50 Circ=89-188cm^2/s Sink radius = .25in
Circ=188cm^2/s
Circ=171cm^2/s
Circ=89cm^2/s
Circulation(cm^2/s)
250
200
150
100
50
0
-150
-100
-50
0
Radius (mm)

Graph 2

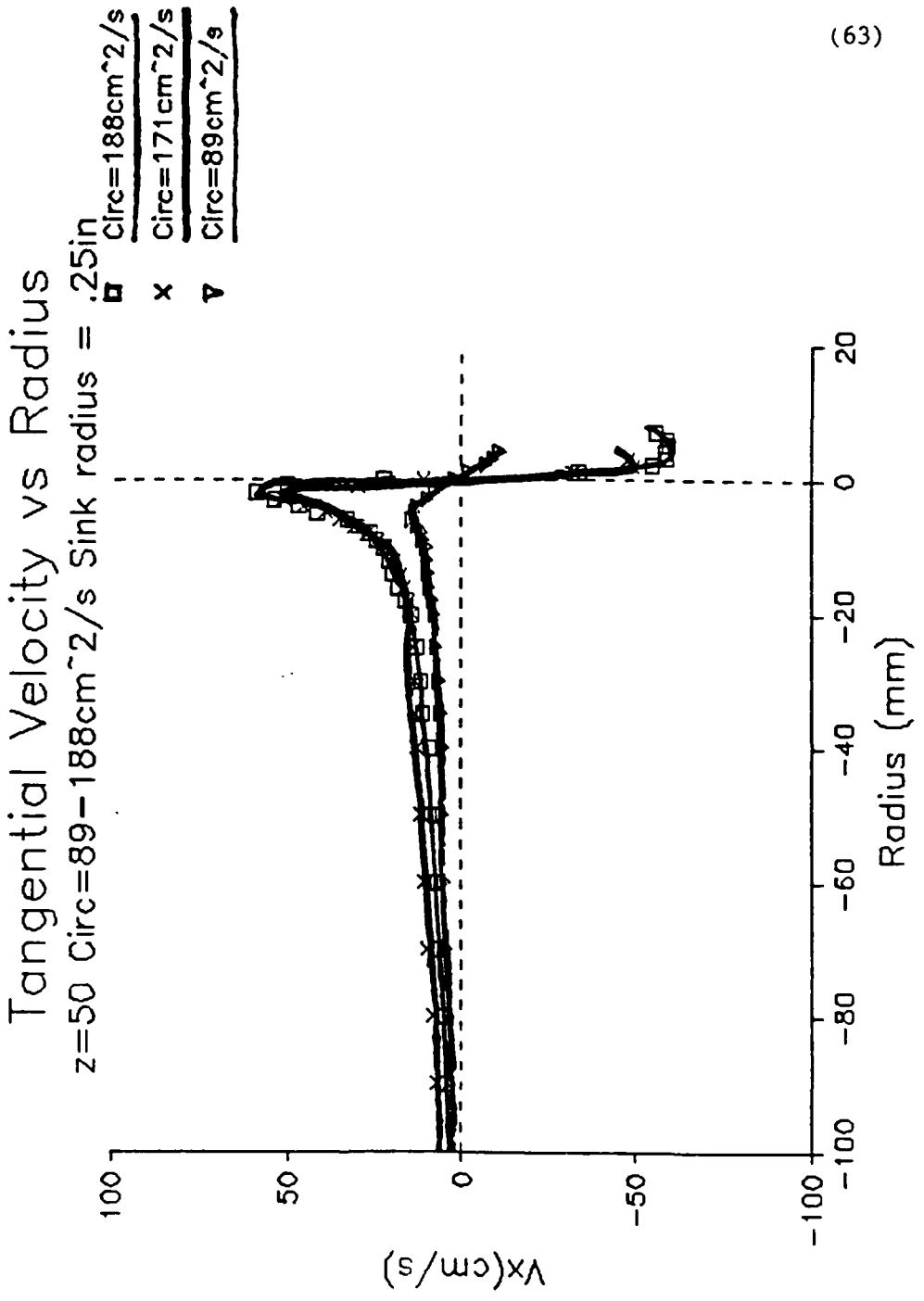
Tangential Velocity vs Radius
z=50 Circ=89-188cm^2/s Sink radius = .25in
Circ=188cm^2/s
Circ=171cm^2/s
Circ=89cm^2/s
Vx(cm/s)
100
50
0
-50
-100
Radius (mm)
20
0
-20
-40
-60
-80
-100

graph 3

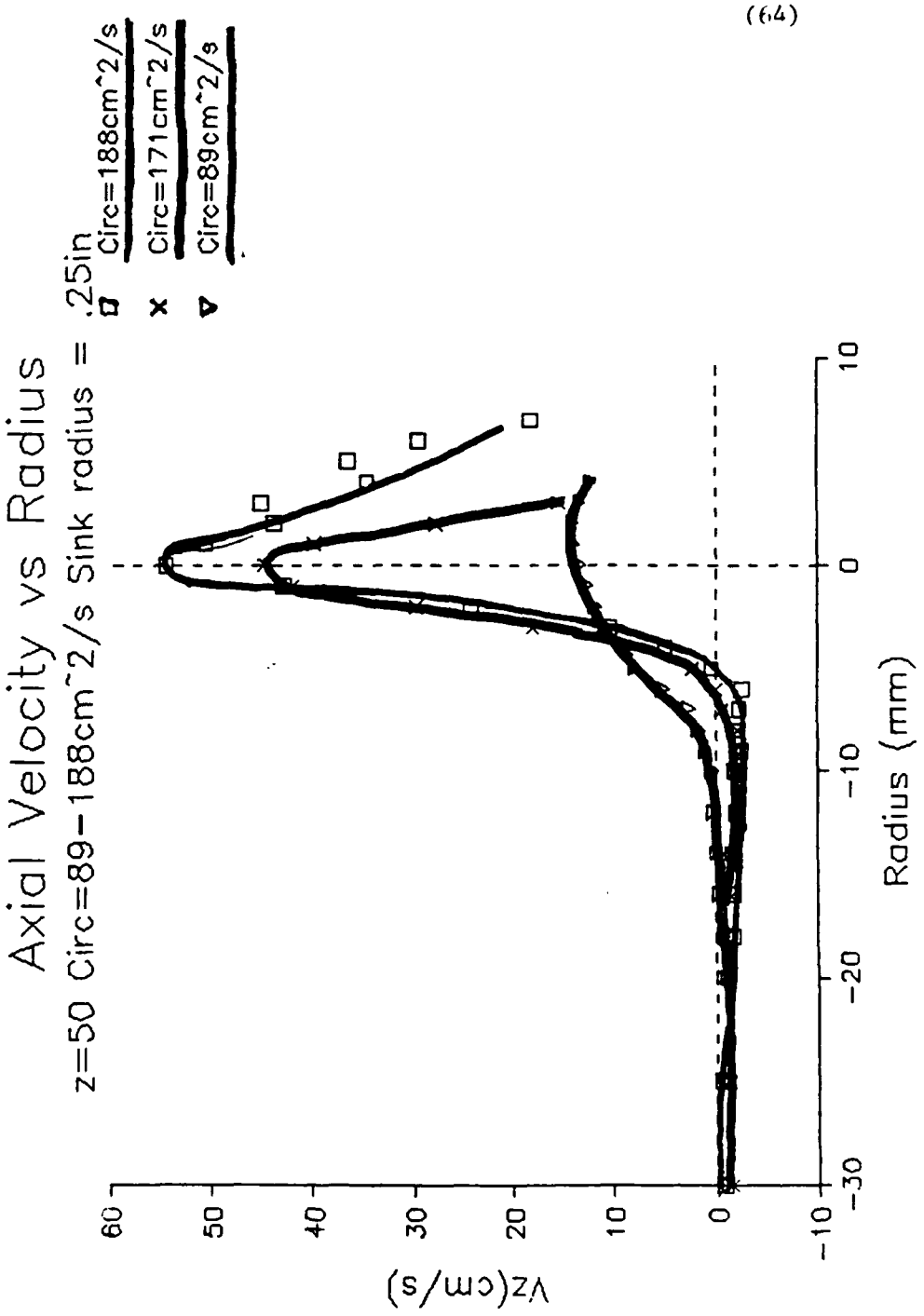
Axial Velocity vs Radius
z=50 Circ=89-188cm^2/s Sink radius = .25in
Circ=188cm^2/s
Circ=171cm^2/s
Circ=89cm^2/s
Vz(cm/s)
60
50
40
30
20
10
0
-10
10
0
-10
-20
-30
Radius (mm)

graph 4

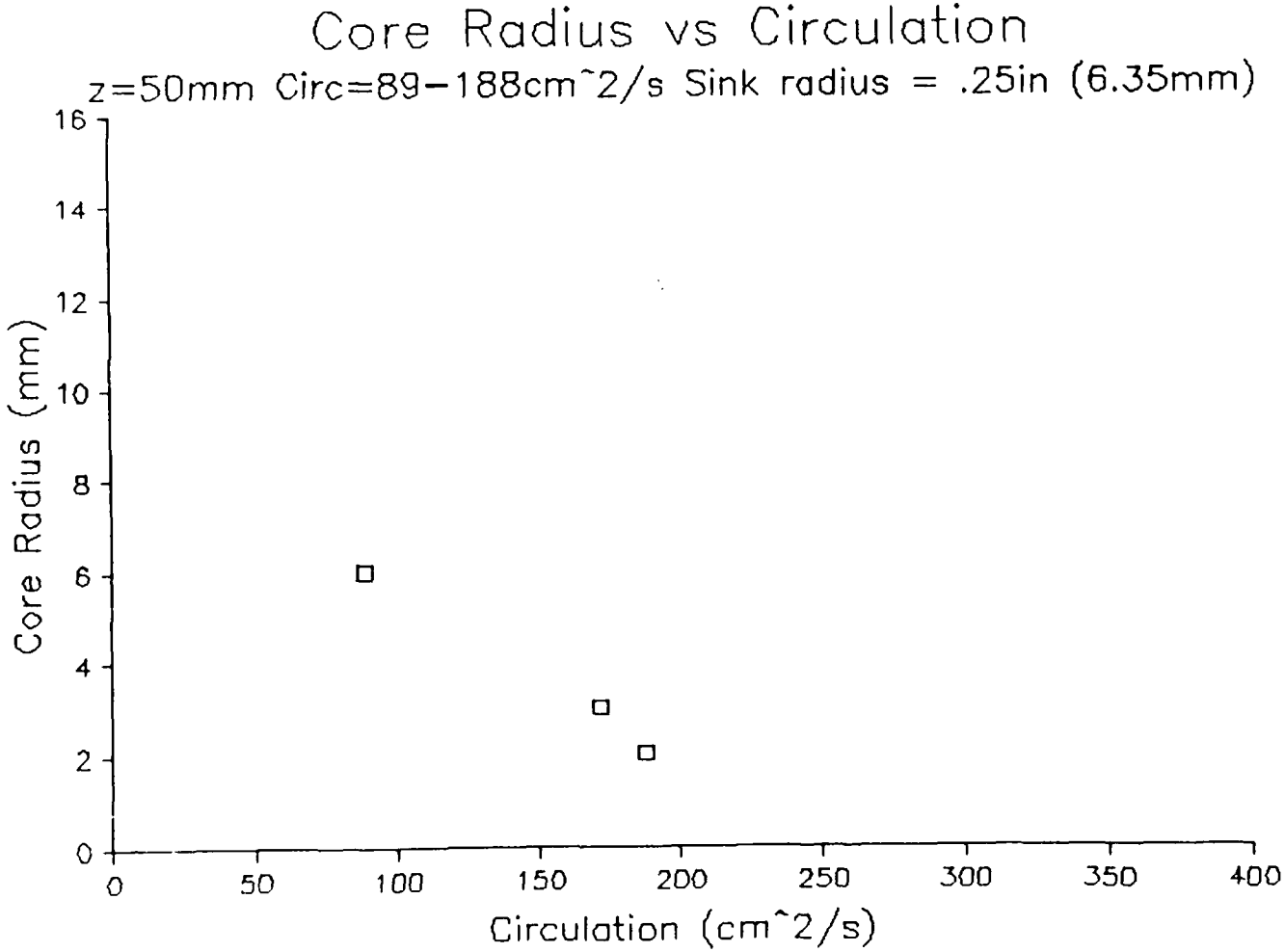
Core Radius vs Circulation
z=50mm Circ=89-188cm^2/s Sink radius = .25in (6.35mm)
Core Radius (mm)
Circulation (cm^2/s)
0
2
4
6
8
10
12
14
16
0
50
100
150
200
250
300
350
400

graph 5

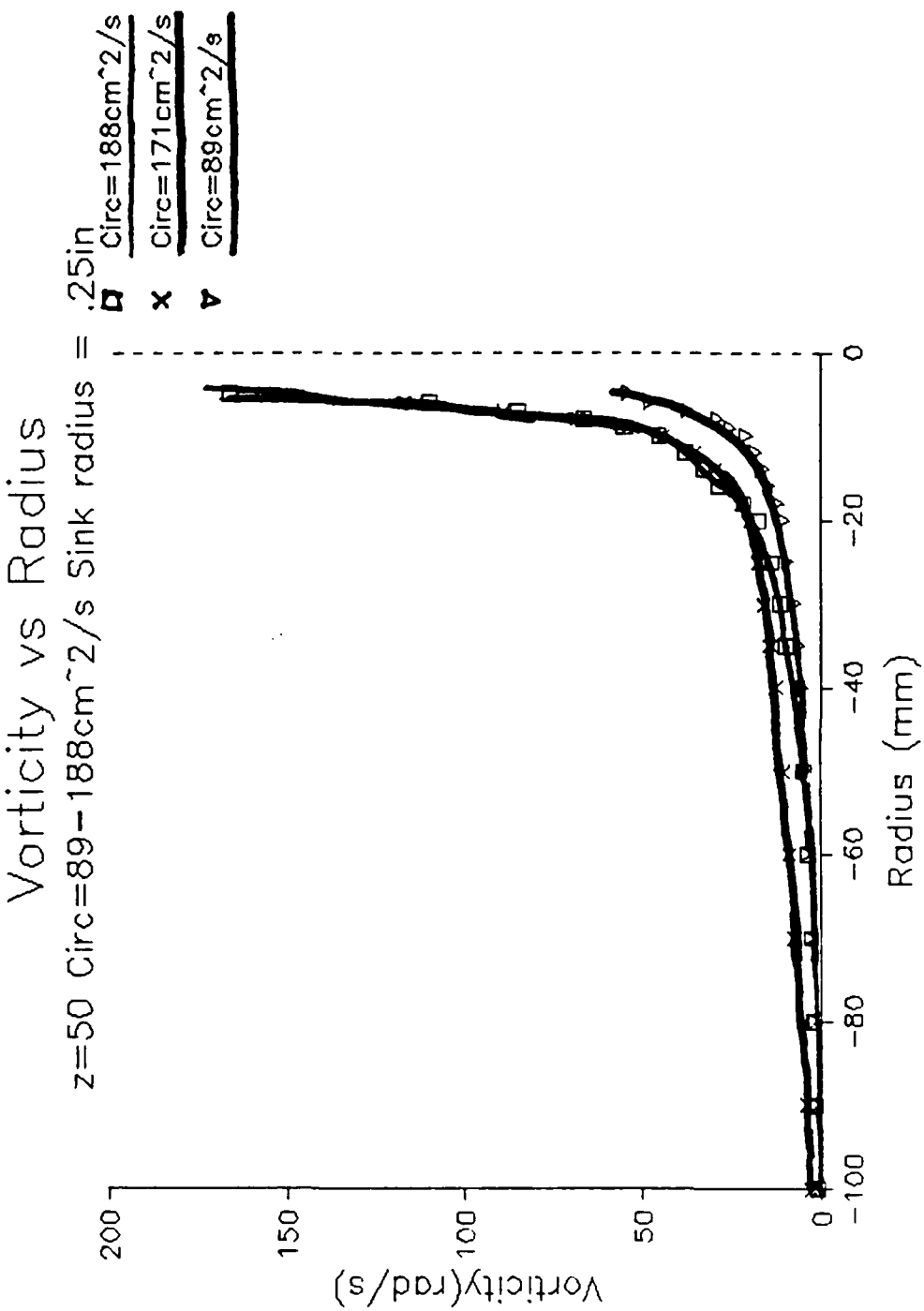
Vorticity vs Radius
z=50 Circ=89-188cm^2/s Sink radius = .25in
Circ=188cm^2/s
Circ=171cm^2/s
Circ=89cm^2/s
Vorticity(rad/s)
200
150
100
50
0
Radius (mm)
0
-20
-40
-60
-80
-100

graph 6

graph 7

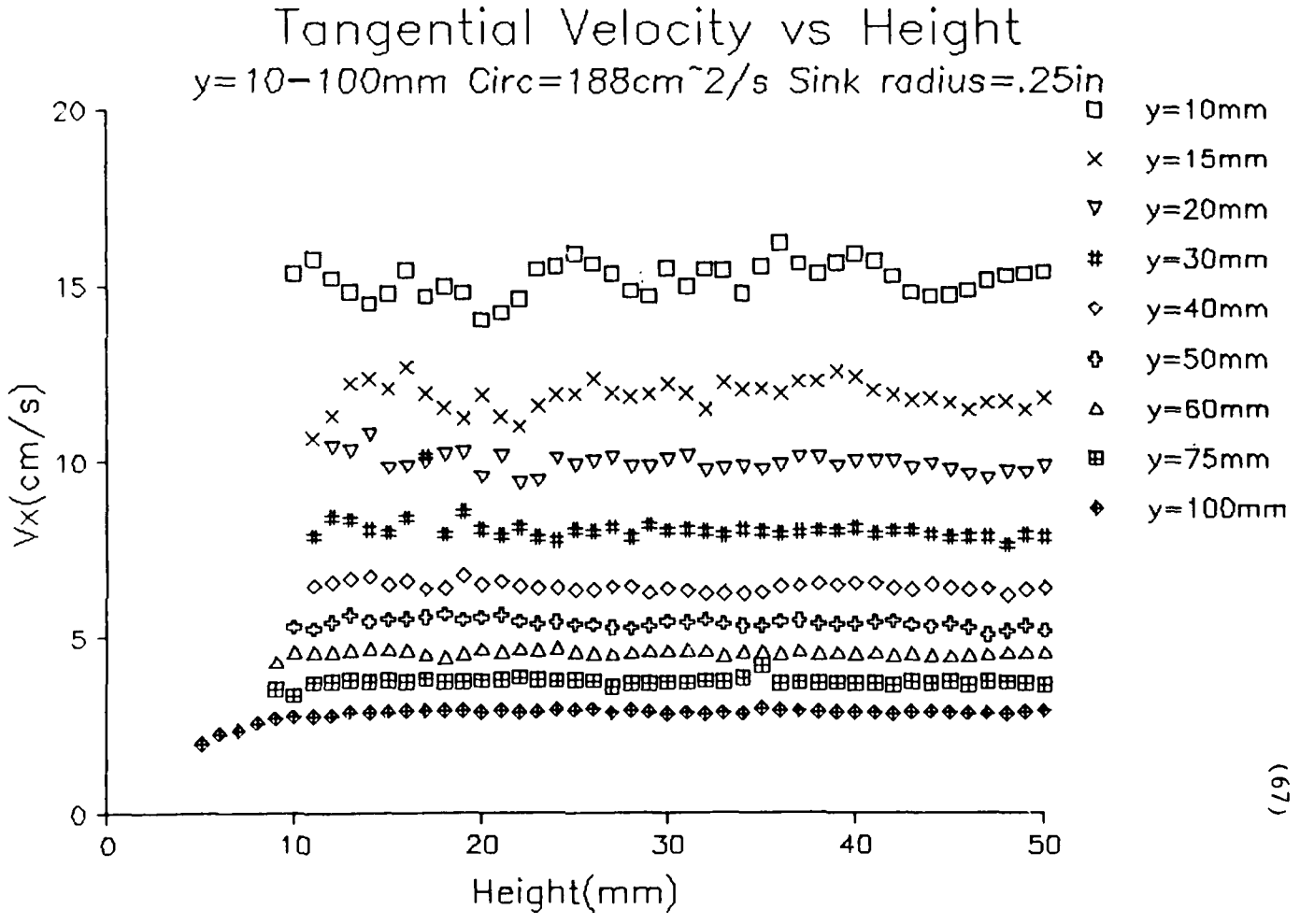
Tangential Velocity vs Height
y=10-100mm Circ=188cm^2/s Sink radius=.25in
Vx(cm/s)
Height(mm)
0
5
10
15
20
0
10
20
30
40
50
y=10mm
y=15mm
y=20mm
y=30mm
y=40mm
y=50mm
y=60mm
y=75mm
y=100mm

graph 8

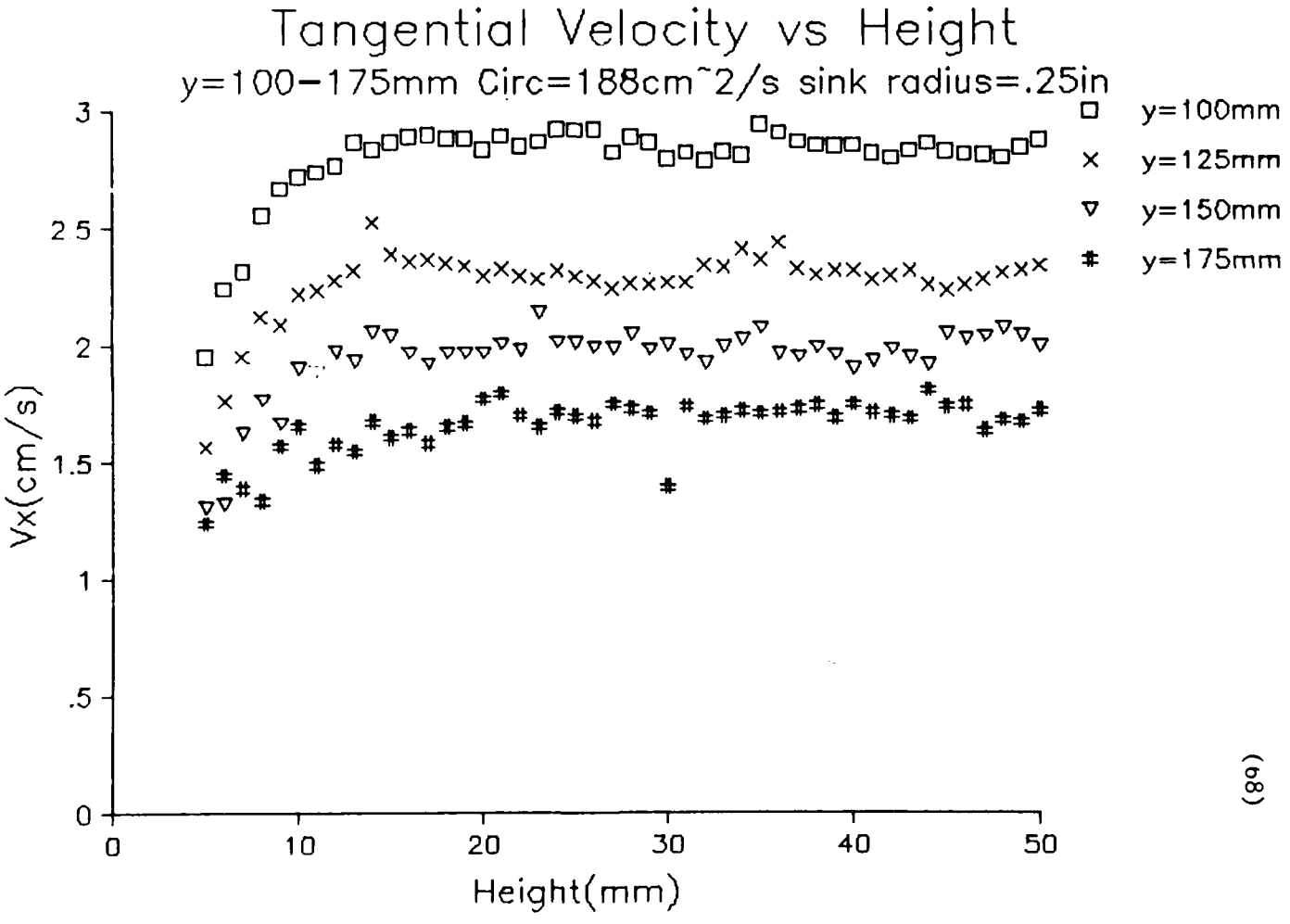
Tangential Velocity vs Height
y=100-175mm Circ=188cm^2/s sink radius=.25in
y=100mm
y=125mm
y=150mm
y=175mm
Vx(cm/s)
Height(mm)
0
.5
1
1.5
2
2.5
3
0
10
20
30
40
50

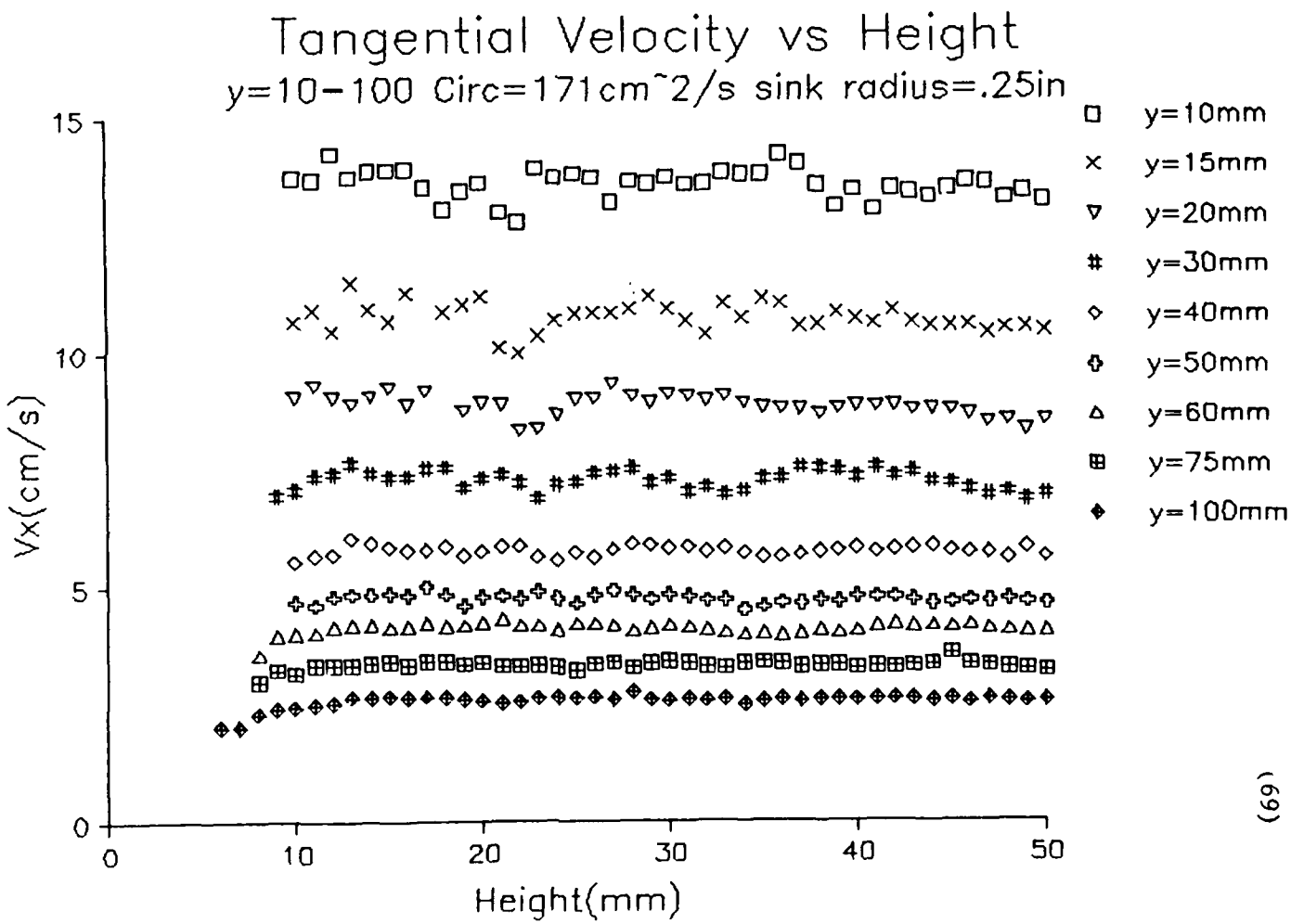
Tangential Velocity vs Height
y=10-100 Circ=171cm^2/s sink radius=.25in
Vx(cm/s)
Height(mm)
0
5
10
15
0
10
20
30
40
50
y=10mm
y=15mm
y=20mm
y=30mm
y=40mm
y=50mm
y=60mm
y=75mm
y=100mm

graph 9

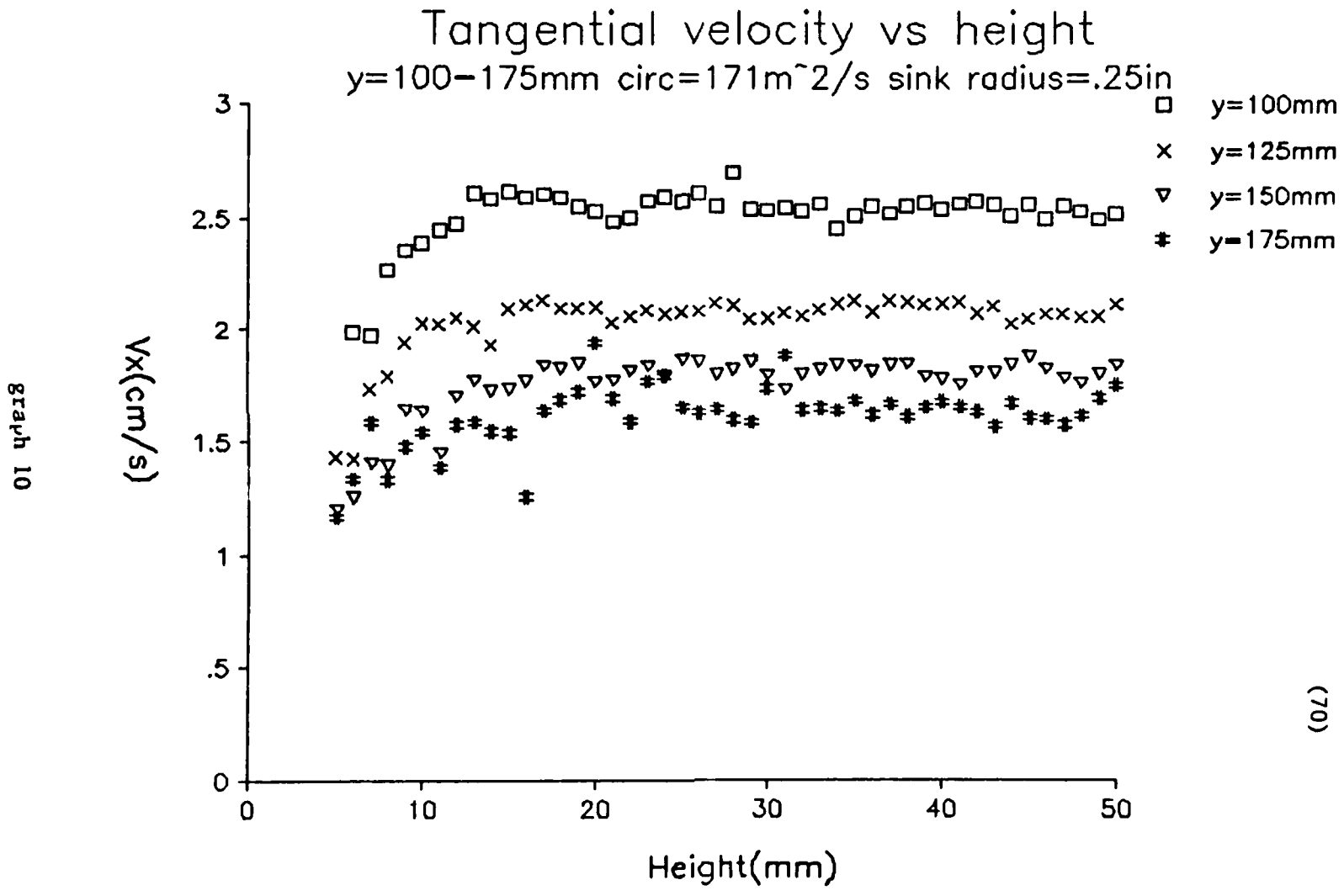
Tangential velocity vs height
y=100-175mm circ=171m^2/s sink radius=.25in
y=100mm
y=125mm
y=150mm
y=175mm
Vx(cm/s)
Height(mm)
0
.5
1
1.5
2
2.5
3
0
10
20
30
40
50

graph 10

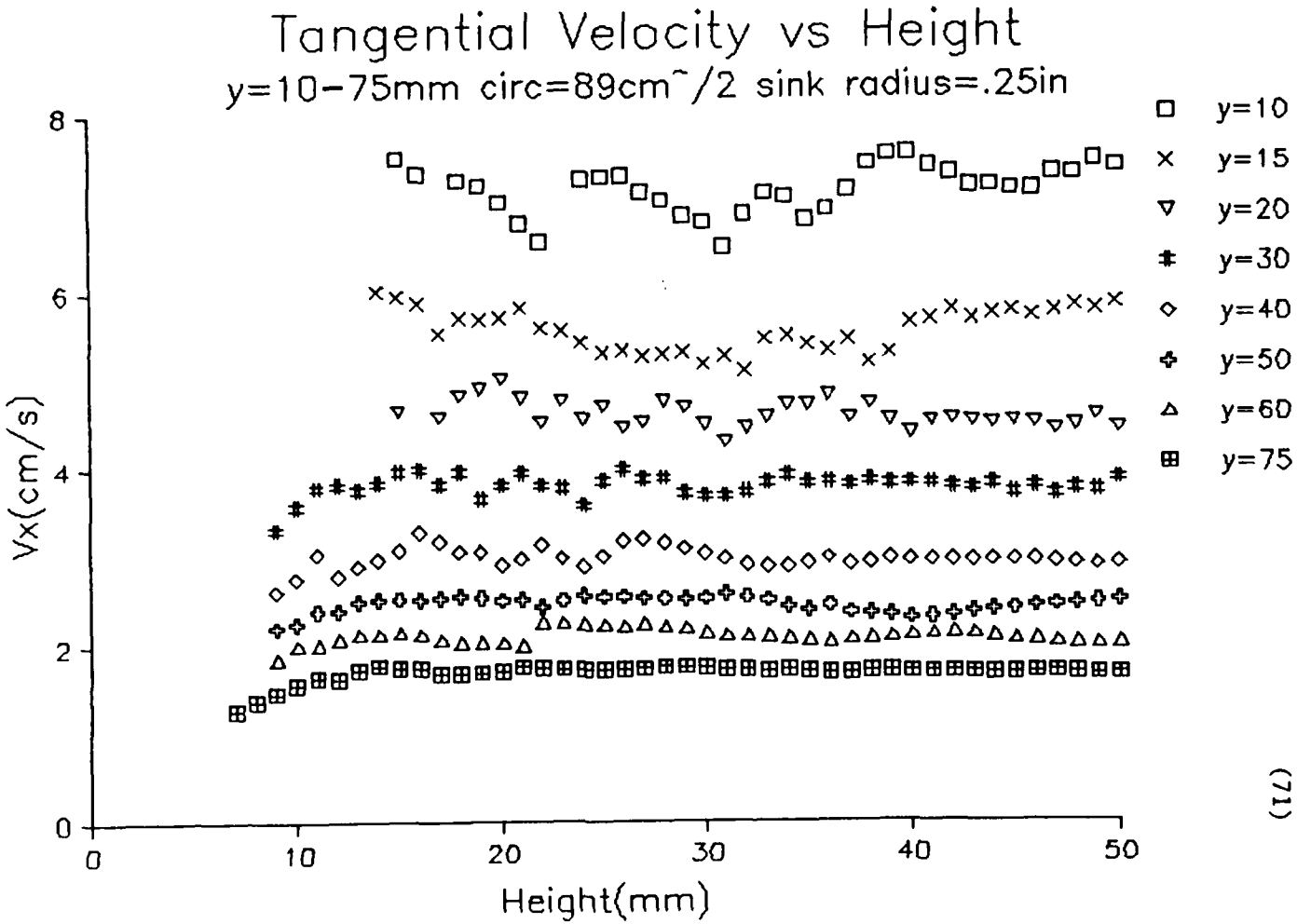
Tangential Velocity vs Height
y=10-75mm circ=89cm^/2 sink radius=.25in
Vx(cm/s)
Height(mm)
0
2
4
6
8
0
10
20
30
40
50
y=10
y=15
y=20
y=30
y=40
y=50
y=60
y=75

graph 11

APPENDIX C (Notes for Future Vortex Investigator)

This Appendix is intended to discuss various aspects of this experimental process. Specific problems that were encountered in the acquisition of a suitable vortex generator, requirements of setup for meaningful results, and problems with the physical behavior of the vortex will be discussed.

The vortex generator for this project was contracted out to Reed Plastics of Washington DC. An extensive delay occurred due to the fact that they were unclear as to what was required, and we were unclear as to what they were capable of producing. The result was that the final vortex generator had to be modified in the machine shop here at USNA in order to get a thick enough window that it would not deflect under pressure. If a new vortex generator is ever ordered, engineering drawings should be done to submit with the purchase order so that the contractor knows what is required and we have a legal basis to require a certain product.

A modification to the present setup should include a flow meter with a much greater accuracy that the one installed at present. The maximum flow rates that could realistically be required are less than three gallons per minute. This project was done with volumetric flow rates under 1.5 gallons per minute.

One problem encountered during this investigation was that a leaky silicone seal between the bottom plate of the vortex generator and the mounting plate. Apparently the loading of the generator and subsequent unloading eventually worked the seal until it failed and water leaked out between the plates. This problem was temporarily solved by using a double bead of silicone in the area around the sink.

It is important that the sink plug be flush mounted with the bottom plate. If the plug extrudes, the flow situation is altered. In this setup, some excess silicone was keeping the plug from fully seating. As a result, some of the flow was entering the gap at the outside edge of the plug, and the boundary layer thickness changed drastically.

If using LDV measurements, it is critical that

the LDV be referenced and aligned correctly to the vortex generator. Not only must the LDV be referenced to some known location, but the axes of traversing must be made to coincide with the axes of the vortex. This is made nearly impossible if the centerline of the vortex is not perfectly rock steady with time as was experienced with this application. The initial alignment for this experimentation was done by placing a steel rod of 1/2 inch diameter inside the sink orifice so that it stuck up vertically. The assumption that the rod was vertical was checked by measuring the distance from the top of the rod to the inner cylinder. If distance was constant, the top of the rod was in the centerline. Since the bottom of the rod was snugly fit in the sink that creates the centerline, the rod was vertical. The LDV measurement volume was placed on the rod and traversed up and down. Jacking screws on the mirror mount table were adjusted until the measuring volume stayed on the rod through a range of axial locations.

The traverse also had to be aligned in the Y direction. Clear plexiglass blocks were used for this.

The blocks were placed at different Y locations and the beam was focused on the top one of them. Jacking screws were adjusted until the beams focused at the same point on each block when the traverse was moved to the Y location. After that, the axial alignment had to be done again because jacking screws affect both to varying degrees. The total reference alignment is then an iterative procedure. If radial velocity measurements are desired, then the iterative procedure becomes immensely more complicated. Radial velocity reference alignment could be relatively simple if Y direction, or tangential velocity alignment is not required.

After the alignment is complete, it is imperative that the experimental setup not be disturbed by cleaning personnel, etc. If it is bumped or knocked, the alignment must be redone.

The bottom and back of the vortex generator was painted flat black in an attempt to reduce the signal to noise ratio in boundary layer measurements. Before the painting was done, specular reflections off the plate and back wall were increasing the noise level in

certain areas of the vortex. After painting, the data rate in some of those areas increased by a factor of three.

After the vortex is filled with water and the motor is turned on, the vortex must be allowed to reach steady state before any measurements have meaning. An experiment was done to determine how long this takes at low valve settings ($\Gamma_\infty < 200$ cm^2/s). The LDV was set to an (X,Y,Z) location of (0,100,100) with appropriate filter settings and a plot of velocity vs time was obtained by reading off velocities from the histogram every ten minutes or so. It takes a vortex approximately 2 hours or so to fully form and reach steady state from stagnant water. If the flow is initiated with a paddle, it takes less time to initially form, but a true steady state requires about 2 hours from any major disturbance.

Seeding was done in order to increase the data rate in the vortex. The seed utilized was silicon carbide #10081 with a particle diameter of 1.5×10^{-6}m. Seeding is essential in this application, as there is an insignificant data rate without it. Seeding

increases the data rate by several orders of magnitude. However, too much seeding can actually decrease data rate. Seeding increases the number of particles that pass through the measurement volume, but it also clouds the water. Beam strength at the measurement volume decreases, and the attenuation of the scattered light increases in cloudier water. A seed mixture of .00228 lb of silicon carbide in 4000 l of water (8.68924 lb) was used to conduct a seeding experiment.

Seed was added in increments of 100 ml. Seed was allowed to fully diffuse before more was added. The data rate for different amounts of seed was determined and the optimum seeding for point (0,100,100) was determined to be between 700 ml and 900 ml. It is possible that some other type of seed may produce better data for this application, but no other seed was available.

APPENDIX D (Notes for Future LDV Operator)

The basic concept of LDV measurements is simple. Two coherent beams of light with the same wavelength will produce a fringe pattern when crossed. This fringe pattern is due to differing amounts of constructive and destructive interference. The space between the fringes can be determined by the wavelength of the light and the geometry of the beams as shown in figure 12 of Appendix A. When a particle in the fluid passes through the measurement volume, it will reflect light. A portion of that light can be collected and focused on a photomultiplier. When the particle passes through a bright spot it reflects much light; when it passes through a dark spot it emits almost none. The current from the photomultiplier that results from this light is represented in figure 12. The peaks of this plot of current vs time correspond to the fringes in space. The velocity of the particle is simply the fringe spacing multiplied

by the frequency of the photomultiplier current.

Where the basic concepts are relatively easy, the technical implementation is exceedingly complex. Everything must be just right to get meaningful data or, indeed, any data at all. The following outline applies to the setup of any LDV experiment.

I. Acquisition of Usable Data

A. Transmitting Optics

1. Must have a beam.

- It was approximately a month before lasing was achieved with the Argon Ion laser used in this project. The back mirror adjustment had somehow previously been forced past its stop. The stop was finally repaired and lasing was achieved. Consult the Lexel model 95A manual for instructions on normal mirror adjustment.
- Present maximum beam power is approximately 1.5 W. It should be up around 3.5 W according to other researchers using the same model laser. Possible solution could be to adjust the front mirror as described in

manual.

- Laser Safety must be observed, including training, permits, medical examination, interlock shutter, and firing log.

2. Alignment

- The laser must be horizontal first. Use the TSI mylar mask at two different locations along track and fine tune the level of the laser. Placement of the mask is critical as well or else the laser will not be truly horizontal or straight. Metal alignment blocks would be much more accurate than the mylar mask, but they would have to be borrowed or carefully made here.
- Each component must have beams proceeding through exactly horizontally and in the right location. No angles can be present in the beam except after the focusing lens. Any misalignment will multiply itself over distance and through other components until the beam is useless.

3. Beam Crossing

- After the entire alignment, the beams will still probably not cross. They can be steered to cross with the steering modules in the color separator. The beam crossing must be checked with a microscope objective that will project the beam crossing area onto a surface such as a screen or wall. A fringe pattern should be visible.

B. Receiving Optics

1. Orifice Alignment in Field Stop

- There is a field stop system that has a pinhole orifice that is designed to keep out extraneous light from a measurement. The scattered light is focused down to a very small area, and the orifice must be placed such that the light from the measurement volume passes through and the other light is blocked. To do this, the measurement volume should be placed on a black surface. The field stop lens must be used to focus the scattered light into the orifice. Then, the X, & Y adjustment screws must be moved to let

the light through the orifice.

- In this experimental procedure, a field stop system was not even used. The field stop was removed to make room for the 3.5 X beam expander. It would be advantageous to have both, but a longer track would be required. A longer track is also desired for the transmitting optics consideration because more open space should follow the acousto-optic modulator to allow cleaner separation of shifted beams.

2. Photomultiplier Tube Alignment

- Again the alignment eyepiece is used to center the pinhole of the photomultiplier on the scattered light focus point. There is another focusing lens that should be used to get the clearest point of light, then the adjustment thumbscrews on the PM tubes should be used to center the point of light on the crosshairs of the alignment eyepiece.
- Fine tuning must be done by observing the burst strength on an Oscilloscope. The eyepiece

will get close, but further adjustment should be done to maximize signal on the Oscilloscope.

- If the PM tube thumbscrews are disturbed or bumped after alignment, signal will probably be lost and a realignment must be done.

C. Signal Processors

1. Shift Requirement

- Frequency shift allows negative velocities to be measured or high velocity flows with a lower range of velocities. It can be thought of as a DC offset to the velocity. What it actually does is shift the frequency of one of the beams so that the fringes are no longer stationary. Moving fringes can read negative velocities or allow high velocities to be read in more accurate ranges.
- In order to know what amount of shift is required, some guesses must be made as to the flow situation. Excessive shift for low velocity flows requires larger filter

settings. Insufficient shift can give spurious data if negative flow is possible.

2. Filter Settings

   - If the current that comes out of the PM tube is put straight into a signal processor without filters, no useful data will come out. The amount of noise over the bandwidth of the PM tube is much greater than the amount of signal from that tiny point far out in your measurement volume. It is possible to get measurements, however, because the current that results from scattered light in the measurement volume has a small bandwidth. Filters are used so that only that range of frequencies that could correspond to particle velocities in the flow being measured will produce data. If high velocities are not expected, filters would be set so that only relatively low frequencies will be passed to the counter processors. Smaller filter settings give greater signal to noise ratios, data rates, number of

measurements possible per point, and therefore, more accurate data. However, small filter bandwidths limit the range of flow that can be observed.

- The most difficult flows to observe, therefore, are flows with a high range of velocities. Flow reversals in tight quarters require large filter settings which add noise.

3. Mode

- The two choices of mode considered in this application were Total Burst Count (TBC), and Continuous. Operating in the TBC mode makes it possible to do a velocity bias correction that accounts for higher velocity particles passing through the measurement volume more frequently than low velocity particles. Continuous mode gives a much higher data rate because it takes more than one measurement per particle burst. However, it does not allow velocity bias correction.
- It was not possible to use the coincidence

mode for this experiment because of the specific optical component setup used. Coincidence mode requires that a signal be present on both components of velocity for a measurement to be recorded. In our optical setup, the measurement volume for the two components did not actually overlap, so this mode could not be used. Our measurement volumes do not overlap because the accusto-optic modulator is used to shift the multicolor beam instead of the beam to be split. This adjustment made the alignment of the optical components easier, but does not allow the coincidence mode to be used. As a result, the experimenter must sit by the counters and adjust gain so that neither counter has a data rate more than about 3 times the other. If this is not done, then one counter will take the majority of data for one position and be very accurate, while the other one gets almost none.

4. Overheating

- Much of the TSI equipment seems to have a problem with overheating. For this application, the counter processors were kept in an electronics rack. Both of the counters began to act sporadically and stopped taking data. One of the counters was replaced with a borrowed one from David Taylor Research Center in Carderock, Maryland. The unreliability was minimized by adding an external fan that blew on the back of the counters.

The following checklist was completed for every laser firing. Used checklists were kept in a 3 ring binder and that served as a firing log.

Date _____ Time emit_____ Time secure _____

Log clock hours WC on _____
slowly open water supply valve
Switch water conditioner on
Check rocker switch glowing
Log flow temperature and pressure Tto_____ Tfrom_____
Get keys for wall breaker and laser
Verify beam attenuator "SHUT"
Unlock wall power station
Verify interlock functional Pto_____ Pfrom_____
Switch wall breaker "ON"
Turn LINE circuit breaker "ON"
Ensure 3 LINE indicators and 3 FUSE indicators lit
Insert key in KEY CONTROL & turn "ON"
Check indicator lights all lit Covers, Water Temp
Water Flow, Reg Temp, and INTLK
Place Laser power meter before beam or shut shutter
Set Control Selector to "Current"
Turn Current Control knob fully clockwise
Switch meter selector to the "Current 50A" position
Press "Power On" pushbutton Log time
Check power indicator lit
Check Laser radiation emission indicators lit
Wait 20-30 seconds
Check Ready indicator lit
Press Laser Start pushbutton to ionize plasma tube
check LASER meter for plasma tube current of 27-33 A
Log plasma tube current Tube current_____
Slide Beam attenuator "open"
Log Beam power Beam power_____

Shutdown

Slide Beam attenuator "Closed"
Press "Power Off" pushbutton Log time
Key control "Off", remove key
Line circuit breakers "OFF"
Wall breaker "Off"
Lock wall breaker
Power off on door Interlock
Wait apx 10 minutes from "power off" or until

Tfrom-Tto = 0
Switch water conditioner "Off"
Close primary water supply valve
Log clock hours WC off _____